Beam polarization effects in the radiative production of lightest neutralinos in e^+e^- collisions in supersymmetric grand unified models

P. N. Pandita[1] and Monalisa Patra[2]

[1]*Department of Physics, North Eastern Hill University, Shillong 793 002, India*
[2]*Centre for High Energy Physics, Indian Institute of Science, Bangalore 560 012, India*
(Received 6 July 2013; published 23 September 2013)

We study the production of the lightest neutralinos in the process $e^+e^- \rightarrow \chi_1^0 \chi_1^0 \gamma$ in supersymmetric grand unified models for the International Linear Collider energies with longitudinally polarized beams. We consider cases where the standard model gauge group is unified into the grand unified gauge groups $SU(5)$, or $SO(10)$. We have carried out a comprehensive study of this process in the $SU(5)$ and $SO(10)$ grand unified theories which includes the QED radiative corrections. We compare and contrast the dependence of the signal cross section on the grand unified gauge group, and on the different representations of the grand unified gauge group, when the electron and positron beams are longitudinally polarized. To assess the feasibility of experimentally observing the radiative production process, we have also considered in detail the background to this process coming from the radiative neutrino production process $e^+e^- \rightarrow \nu \bar{\nu} \gamma$ with longitudinally polarized electron and positron beams. In addition we have also considered the supersymmetric background coming from the radiative production of scalar neutrinos in the process $e^+e^- \rightarrow \tilde{\nu} \tilde{\nu}^* \gamma$ with longitudinally polarized beams. The process can be a major background to the radiative production of neutralinos when the scalar neutrinos decay invisibly.

I. INTRODUCTION

In supersymmetric models with R parity (R_P) conservation, the lightest neutralino is expected to be the lightest supersymmetric particle (LSP). Because of R_P conservation, the lightest neutralino is absolutely stable. Being the LSP, it is the end product of any process that involves supersymmetric particles in the final state. Because of its importance in supersymmetric phenomenology, there have been extensive studies of the neutralino sector of the minimal supersymmetric standard model (MSSM) [1] and its extensions [2–10]. The discovery of neutralinos is one of the main goals of present and future accelerators. In particular, an e^+e^- collider with a center-of-mass energy of $\sqrt{s} = 500$ GeV in the first stage will be an important tool in determining the parameters of the underlying supersymmetric model with a high precision [11–15] The capability of such a linear collider in unravelling the structure of supersymmetry (SUSY) can be enhanced by using polarized electron and positron beams [16].

When the standard model (SM) gauge symmetry $SU(2) \times U(1)$ is broken, the fermionic partners of the two Higgs doublets (H_1, H_2) of the MSSM mix with the fermionic partners of gauge bosons, resulting in four neutralino states $\tilde{\chi}_i^0$, $i = 1, 2, 3, 4$, and two chargino states $\tilde{\chi}_j^\pm$, $j = 1, 2$. The composition and mass of the lightest neutralino, which depends on the soft $SU(2)$ and $U(1)$ gaugino masses, M_2 and M_1, on the Higgs(ino) parameter, μ, and on the ratio of the two Higgs vacuum expectation values, $\tan \beta \equiv v_2 / v_1$, will be crucial for the search for supersymmetry at the colliders. The values of the soft gaugino masses at the electroweak scale depend on the boundary conditions on these masses at the grand unified theory (GUT) scale. In most of the studies, the gaugino masses have been taken to be universal at the GUT scale. However, there is no particular reason to assume that the soft gaugino masses are universal at the high scale. Indeed, it is possible to have nonuniversal soft gaugino masses in grand unified theories. We recall that soft supersymmetry gaugino masses are generated from higher-dimensional interaction terms involving gauginos and auxiliary parts of chiral superfields [17]. For example, in $SU(5)$ grand unified theory, the auxiliary part of a chiral superfield in higher-dimensional terms can be in the representation **1**, **24**, **75**, or **200** or, in general, some combination of these representations.

When the auxiliary field of one of the $SU(5)$ nonsinglet chiral superfields obtains a vacuum expectation value (VEV), then the resulting gaugino masses are nonuniversal at the grand unification scale. Similar conclusions hold for other supersymmetric grand unified models. Furthermore, nonuniversal supersymmetry breaking masses are a generic feature in some of the realistic supersymmetric models. For example, in anomaly mediated supersymmetry breaking models, the gaugino masses are not unified [18,19] and hence are not universal.

From the above discussion, it is clear that the phenomenology of supersymmetric models depends crucially on the composition of neutralinos and charginos. This in turn depends on the soft gaugino mass parameters M_2 and M_1, besides the parameters μ and $\tan \beta$. Since most of the models discussed in the literature assume gaugino mass universality at the GUT scale, it is important to investigate the changes in the phenomenology of broken supersymmetry which results from the changes in the composition of

neutralinos and charginos that may arise because of the changes in the pattern of soft gaugino masses at the grand unification scale [20]. The consequences of nonuniversal gaugino masses at the grand unified scale and the resulting change in boundary conditions has been considered in several papers. This includes the study of constraints arising from different experimental measurements [21–23] and in the study of supersymmetric dark matter candidates [24,25].

Recently in Refs. [26,27] a detailed study of the radiative production of neutralinos in electron-positron collisions in low-energy supersymmetric models with universal gaugino masses at the grand unified scale was carried out. Furthermore, we have carried out a detailed study of the radiative production of the lightest neutralinos in electron-positron collisions in grand unified theories [28]. Since longitudinal beam polarization is going to play a crucial role in electron-positron collisions, it is important to study its effects on the radiative production of the lightest neutralinos in electron-positron colliding beam experiments in the case of grand unified theories.

In this paper we shall carry out a detailed study of the implications of the nonuniversal gaugino masses, as they arise in grand unified theories, for the production of lightest neutralinos in electron-positron collisions with longitudinally polarized beams. Our purpose is to study the role of longitudinal beam polarization as a probe of supersymmetric grand unified theories. For this purpose we shall consider the case of $SU(5)$ and $SO(10)$ grand unified theories, these being the typical ones wherein the standard model can be embedded in a grand unified gauge group. The motivation of this comes from the fact that longitudinal beam polarization is a distinct possibility at the International Linear Collider (ILC). Studies of this type have not been carried out so far in the context of grand unified theories. Since in a large class of models of supersymmetry the lightest neutralino is expected to be the lightest supersymmetric particle, it will be one of the first states to be produced at the colliders, even if other SUSY particles may be too heavy to be produced. Moreover, this process is likely to complement the search of the SUSY spectrum at the LHC, where the squarks and gluinos are likely to be produced and studied in detail. The radiative neutralino production at the ILC will, thus, be an independent study irrespective of whether the colored sparticles are found at the Large Hadron Collider. A detailed study of this process at the ILC will let us determine the mass and composition of the lightest neutralino along with its couplings, which by itself would be an important advance. The experimental performance of the radiative neutralino production along with the neutralino mass measurement have been recently evaluated in a full detector simulation for the international large detector [29]. At an electron-positron collider, such as the ILC, the lightest neutralino can be directly produced in pairs [3,30]. However, it will escape detection such that the direct production of the lightest neutralino pair is invisible. One can, however, look for the

signature of neutralinos in electron-positron colliders in the radiative production process,

$$e^+ + e^- \rightarrow \tilde{\chi}_1^0 + \tilde{\chi}_1^0 + \gamma. \tag{1.1}$$

The signature of this process is a single high-energy photon with missing energy carried away by the neutralinos. In this paper we carry out a detailed study of the process (1.1) in supersymmetric grand unified theories with nonuniversal boundary conditions at the grand unified scale with polarized electron and positron beams. The process (1.1) has been studied in detail in the minimal supersymmetric model [31–41], in various approximations. Calculations have also been carried out for the MSSM using general neutralino mixing [39–41]. This process has also been studied in detail in the next-to-minimal supersymmetric model [26,27]. On the other hand, different large electron positron collider (LEP) collaborations [42–46] have studied the signature of radiative neutralino production in detail but have found no deviations from the SM prediction. Thus, they have only been able to set bounds on the masses of supersymmetric particles [42–44,46]. Also, the role of longitudinal polarization for process (1.1) has been studied in [47].

We recall here that in the SM the radiative neutrino process

$$e^+ e^- \rightarrow \nu + \bar{\nu} + \gamma \tag{1.2}$$

is the leading process with the same signature as Eq. (1.1). The cross section for the process (1.2) depends on the number N_ν of light neutrino species [48]. This process acts as a main background to the radiative neutralino production process (1.1). Furthermore, there is also a supersymmetric background to the process (1.1) coming from radiative sneutrino production:

$$e^+ e^- \rightarrow \tilde{\nu} + \tilde{\nu}^* + \gamma. \tag{1.3}$$

We shall consider both these processes, since they form the main background to the radiative process (1.1) and are important for determining the feasibility of observing the radiative production of lightest neutralinos in electron-positron collisions.

For the signal process (1.1), the dominant SM background process (1.2) proceeds through the exchange of W bosons, which couple only to left-handed particles. At the LEP this dominant background process made it impossible to see the possible signal of the radiative process (1.1), even for very light neutralinos. Furthermore, in the case of the LHC, a search has been made for the final states in pp collisions, containing a photon (γ) of large transverse momentum and missing energy. These events can be produced by the underlying reaction $q\bar{q} \rightarrow \gamma \chi \bar{\chi}$, where the photon is radiated by one of the incoming quarks and where χ is a dark matter candidate (possibly the lightest neutralino). The primary background for such a signal at the LHC is the irreducible SM background from $Z\gamma \rightarrow \nu\bar{\nu}\gamma$. This and other SM backgrounds were taken into account in the

LHC analysis. The observed number of events was found to be in agreement with the SM expectations for the γ + missing energy events. From this an upper limit for the production of χ in the γ + missing transverse energy state was obtained [49]. In view of these negative results, the International Linear Collider, with the possibility of beam polarization, will be a good place to look for the process with an energetic photon and large missing energy in the final state characteristic of the reaction (1.1). Furthermore, in the case of the ILC with the possibility of polarized electron and positron beams, a suitable choice of beam polarization ($e_R^- e_L^+$) will significantly reduce the SM background.

The layout of the paper is as follows. In Sec. II, we discuss the constraints on the supersymmetric particle spectrum arising from the experimental results from the LHC, the Tevatron, and the LEP. In Sec. III, we implement the constraints on the parameter space of the grand unified models as they arise from the constraints on the super-symmetric particle spectrum discussed in Sec. II. Here we also calculate the elements of the mixing matrix which are relevant for obtaining the couplings of the lightest neutra-lino to the electron, selectron, and Z boson which control the radiative neutralino production process (1.1). We also describe in detail the typical set of input parameters that is used in our numerical evaluation of cross sections. The set of parameters that we use is obtained by imposing various experimental and theoretical constraints discussed in Sec. II on the parameter space of the minimal supersym-metric standard model with underlying grand unification. These constraints will be used throughout to arrive at the allowed parameter space for different models in this paper. Furthermore, in Appendix A we briefly review different patterns of gaugino masses that arise in grand unified theories. Here we will consider grand unified theories based on $SU(5)$ and $SO(10)$ gauge groups and outline the origin of nonuniversal gaugino masses for these models.

In Sec. IV, we summarize the cross section for the signal process, including the beam polarization and its implica-tions for the signal cross section. Here we also describe in detail the effect of QED radiative corrections on the cross section for the radiative neutralino production cross sec-tion. In Sec. V, we evaluate the cross section for the signal process (1.1) in different grand unified theories with non-universal gaugino masses, using the set of parameters obtained in Sec. III for different patterns of gaugino mass parameters at the grand unified scale. We have included higher-order QED radiative corrections, as described in Sec. IV, in all our calculations. We also compare and contrast the results so obtained with the corresponding cross section in the MSSM with universal gaugino masses at the grand unified scale. The dependence of the cross section on the parameters of the neutralino sector and on the selectron masses is also studied in detail.

In Sec. VI we discuss the backgrounds to the radiative neutralino production process (1.1) from the SM and supersymmetric processes. An excess of photons from radiative neutralino production, with the longitudinally polarized electron and positron beam, over the backgrounds measured through statistical significance is also discussed here and calculated for different grand unified models. We summarize our results and conclusions in Sec. VII.

II. EXPERIMENTAL CONSTRAINTS

In this section, we discuss the latest constraints on the SUSY particle spectrum from the data from the Large Hadron Collider, along with the data from the Tevatron and LEP. At the LHC the search for the SUSY particles is carried through different channels and with different final states. The final states can contain jets, isolated leptons, and E_T^{miss} or will have same-sign dileptons or jets with high p_T. Different final states are considered to increase the sensitivity to a different SUSY spectrum. Observations at the LHC are in good agreement with the SM expectation; therefore, constraints have been set on the cross sections for the SUSY processes. Interpreted differently since no supersymmetric partners of the SM have been detected, lower limits are obtained on their masses.

A. Limits on gaugino mass parameters

The lightest chargino mass and field content is sensitive to the parameters M_2, μ, and $\tan\beta$. At the LEP the search for the lightest chargino through its pair production has yielded a lower limit on its mass [50]. The limits obtained depend on the mass of the sfermions. For the chargino masses following from nonobservation of chargino pair production in e^+e^- collisions at the LEP, we have the constraint

$$M_{\tilde{\chi}_1^\pm} \gtrsim 103 \text{ GeV}. \tag{2.1}$$

The limit depends on the sneutrino mass. For a sneutrino mass below 200 GeV, the bound becomes weaker, since the production of a chargino pair becomes more rare due to the destructive interference between γ or Z in the s channel and $\tilde{\nu}$ in the t channel. In the models we consider, $m_{\tilde{\nu}}$ is close to m_0, where m_0 is the soft SUSY breaking scalar mass. When $m_{\tilde{\nu}} < 200 \text{ GeV}$, but $m_{\tilde{\nu}} > m_{\tilde{\chi}^\pm}$, the lower limit becomes [51]

$$M_{\tilde{\chi}_1^\pm} \gtrsim 85 \text{ GeV}. \tag{2.2}$$

For the parameters of the chargino mass matrix, the limit (2.1) implies an approximate lower limit [52,53]:

$$M_2, \qquad \mu \gtrsim 100 \text{ GeV}. \tag{2.3}$$

The lower limits in Eq. (2.3) on M_2 and μ are obtained by scanning over the MSSM parameter space and are, there-fore, expected to be model independent [10]. Recently a search was done by the ATLAS experiment for the direct production of charginos and neutralinos in the final states with three leptons and p_T^{miss}. In the context of simplified models, degenerate $\tilde{\chi}_1^\pm$ and $\tilde{\chi}_2^0$ with masses up to 300 GeV are excluded for large mass differences with the $\tilde{\chi}_1^0$. For our

analyses we have considered the limit set on the chargino mass from the LEP. The combination of chargino, slepton, and Higgs boson searches has provided a lower limit on $m_{\tilde{\chi}_1^0}$ as a function of $\tan\beta$. The absolute lower limit on the neutralino mass is 47 GeV at large $\tan\beta$.

B. Exclusion limits on squarks and gluinos

The colored SUSY particles, being QCD-mediated processes, can be more copiously produced in the proton-(anti)proton collider with their higher center-of-mass energies compared to the LEP. In the context of the constrained supersymmetric standard model (CMSSM), Tevatron experiments have excluded squark and gluino masses of 379 and 308 GeV, respectively, based on an integrated luminosity of 2.1 fb^{-1}.

In the framework of the CMSSM, the LHC experiments with approximately 5 fb^{-1} of data have excluded gluino masses below 800 GeV for all squark masses. Moreover, squark and gluino masses below approximately 1400 GeV are excluded at 95% C.L. (for equal squark and gluino masses) [54,55]. The limits, though derived for a particular choice of parameters in the context of CMSSM, depend slightly on the choice. Analyses have also been done setting a limit on gluino mass as a function of the lightest neutralino. The limits obtained are sensitive to the neutralino mass and to the gluino neutralino mass difference.

In the framework of the CMSSM, the LHC experiments have also obtained limits on the first- and second-generation squark masses [54,55]. They have excluded masses below around 1300 GeV for all values of gluino masses. Similarly, an analysis is carried out on the squark mass as a function of the neutralino mass. Overall, considering all the analyses carried out by LHC in the context of different models, first- and second-generation squarks along with the gluinos are excluded with masses below 1200 GeV.

The limits on the third-generation squark $\tilde{t}_1$ mass from the LEP is around 96 GeV, in the charm plus neutralino final state [50]. Experiments at the LHC and at Tevatron have performed the analyses for third-generation squarks in different scenarios, leading to different final states [56]. Similar analyses have been carried out for the sbottom quarks. Overall, for our analyses we will consider the scenario where the third-generation squarks are excluded below a mass of about 800 GeV.

C. Exclusion limit on slepton masses

The limits on the selectrons, smuons, and staus masses are from the LEP experiments [50] because of its clean

signature. The limits obtained on the sleptons are sensitive to the lightest neutralino mass. The smuons and staus with masses below 95 GeV are excluded depending on the lightest neutralino ($\tilde{\chi}_1^0$) mass, provided the mass difference of the slepton and ($\tilde{\chi}_1^0$) is less than 7 GeV. A lower limit of around 73 GeV is set on the mass of the right-handed selectron, $m_{\tilde{e}_R}$, independent of the neutralino mass.

A lower limit of around 45 GeV is obtained on the sneutrino mass from the measurement of the invisible Z decay width. In the context of the MSSM, tighter limits are obtained on the mass of sneutrino of around 94 GeV, assuming gaugino mass universality at the GUT scale.

Taking into account all the constraints set by the different experiments as detailed above, for our analyses we have considered $m_{\tilde{g}} \approx 1400$ GeV, masses of first two generation squarks ≈ 1300 GeV, the third-generation squarks $m_{\tilde{t},\tilde{b}}$ around 1000 GeV, and the slepton of mass around 150 GeV. For the lightest chargino and neutralino, the LEP limit is respected since it gives more stringent bounds compared to the LHC. The Higgs mass is taken to be consistent with the present LHC results.

III. COMPOSITION OF THE LIGHTEST NEUTRALINOS IN GRAND UNIFIED THEORIES

In this section we list the set of parameters used for our analysis along with the composition of the lightest neutralino in grand unified theories. In Appendix A we review the patterns of nonuniversal gaugino masses in grand unified theories. For the sake of completeness, we have first considered the case of universal gaugino masses in supersymmetric theories. In Appendix B we summarize our notations for the neutralino mass matrix and the interaction vertices relevant for our study [57].

We have used the set of parameters listed in Table I for our analysis in the case of universal gaugino masses at the grand unified scale. The values of the parameters are chosen so as to satisfy the various experimental constraints listed in Sec. II. We have restricted ourselves to a particular choice of parameter set with the values of M_2 and μ chosen to correspond to a lightest neutralino of mass around 108 GeV. The reason for the choice of this set was discussed in Ref. [28]. We call this set of parameters the MSSM electroweak symmetry breaking (EWSB) scenario [58]. In this scenario we can study the dependence of the neutralino masses as well as the radiative neutralino production cross section on μ, M_2, and the selectron masses.

TABLE I.   Input parameters and resulting masses of various states in the MSSM EWSB scenario.

$\tan\beta = 10$	$\mu = 130$ GeV	$M_1 = 197$ GeV	$M_2 = 395$ GeV
$M_3 = 1402$ GeV	$A_t = 2800$ GeV	$A_b = 2800$ GeV	$A_\tau = 1000$ GeV
$m_{\tilde{\chi}_1^0} = 108$ GeV	$m_{\tilde{\chi}_1^\pm} = 125$ GeV	$m_{\tilde{e}_R} = 156.2$ GeV	$m_{\tilde{\nu}_e} = 136$ GeV
$m_{\tilde{\chi}_2^0} = 140$ GeV	$m_{\tilde{\chi}_2^\pm} = 421.7$ GeV	$m_{\tilde{e}_L} = 156.7$ GeV	$m_h = 125.7$ GeV

The composition of the lightest neutralino in case of the MSSM EWSB scenario for the parameters of Table I is given by

$$N_{1j} = (0.348, -0.175, 0.702, -0.595). \qquad (3.1)$$

Thus, the lightest neutralino has a dominant Higgsino component. The couplings of the lightest neutralino to electrons, selectrons, and Z bosons are listed in Table XVII of Appendix B. From this table it is clear that for a neutralino with composition (3.1), the neutralino—Z^0 coupling is enhanced compared to the coupling of the lightest neutralino with right and left selectrons $\tilde{e}_{R,L}$.

For our analyses, as a benchmark we have used the radiative neutralino cross section for the MSSM EWSB scenario with the set of parameters as shown in Table I.

The input parameters and the resulting masses for the **24**-, **75**-, and **200**-dimensional representations of $SU(5)$ which result in nonuniversal gaugino masses at the grand unified scale obtained in a manner described later in Appendix A 2 are shown in Tables II, III, and IV, respectively. In arriving at the parameter values in these tables, we have taken into account various theoretical and phenomenological constraints, including the electroweak symmetry breaking at the correct scale, as described in the Sec. II. Other values can be obtained by choosing larger values of the parameter M_3.

The composition of the lightest neutralino for the different representations of $SU(5)$ in Table XIII is obtained from the mixing matrix for the choices of parameters given in Tables II, III, and IV. This composition is calculated to be:

(1) $SU(5)$ with Φ and F_Φ in the **24**-dimensional representation (labelled as model $[SU(5)]_{24}$):

$$N_{1j} = (0.643, -0.053, 0.596, -0.479); \qquad (3.2)$$

(2) $SU(5)$ with Φ and F_Φ in the **75**-dimensional representation (labelled as model $[SU(5)]_{75}$):

$$N_{1j} = (0.031, 0.056, -0.712, -0.700); \qquad (3.3)$$

(3) $SU(5)$ with Φ and F_Φ in the **200**-dimensional representation (labelled as model $[SU(5)]_{200}$):

$$N_{1j} = (0.018, -0.085, 0.719, -0.689). \qquad (3.4)$$

We note from Eqs. (3.2), (3.3), and (3.4) that for the **24**-dimensional representation of $SU(5)$, the dominant component of the neutralino is the bino, whereas for the other representations of $SU(5)$, there is a Higgsino-like lightest neutralino. Thus, for **75**- and **200**-dimensional representations, the neutralino, being Higgsino-like, couples weakly to the selectron, with the dominant contribution to the cross section coming from the neutralino-Z^0 coupling.

Similarly in the case of $SO(10)$, for the parameters of Tables V, VI, and VII, the composition of the lightest neutralino is given by the following:

TABLE II.   Input parameters and resulting masses for various states in $SU(5)$ supersymmetric grand unified theory with Φ and F_Φ in the **24**-dimensional representation. We shall refer to this model as $[SU(5)]_{24}$ in the text.

$\tan\beta = 10$	$\mu = 138$ GeV	$M_1 = 149$ GeV	$M_2 = 890$ GeV
$M_3 = -2121$ GeV	$A_t = -1000$ GeV	$A_b = -2700$ GeV	$A_\tau = -2700$ GeV
$m_{\chi_1^0} = 108$ GeV	$m_{\chi_1^\pm} = 138.7$ GeV	$m_{\tilde{e}_R} = 156$ GeV	$m_{\tilde{\nu}_e} = 136$ GeV
$m_{\chi_2^0} = 146$ GeV	$m_{\chi_2^\pm} = 905$ GeV	$m_{\tilde{e}_L} = 157$ GeV	$m_h = 124$ GeV

TABLE III.   Input parameters and resulting masses for various states in $SU(5)$ supersymmetric grand unified theory with Φ and F_Φ in the **75**-dimensional representation. We shall refer to this model as $[SU(5)]_{75}$ in the text.

$\tan\beta = 10$	$\mu = 108$ GeV	$M_1 = -993.9$ GeV	$M_2 = 1172$ GeV
$M_3 = 1401$ GeV	$A_t = 1000$ GeV	$A_b = 2700$ GeV	$A_\tau = 3000$ GeV
$m_{\chi_1^0} = 108$ GeV	$m_{\chi_1^\pm} = 109$ GeV	$m_{\tilde{e}_R} = 156$ GeV	$m_{\tilde{\nu}_e} = 136$ GeV
$m_{\chi_2^0} = 112$ GeV	$m_{\chi_2^\pm} = 1180$ GeV	$m_{\tilde{e}_L} = 157$ GeV	$m_h = 125$ GeV

TABLE IV.   Input parameters and resulting masses for various states in $SU(5)$ supersymmetric grand unified theory with Φ and F_Φ in the **200**-dimensional representation. We shall refer to this model as $[SU(5)]_{200}$ in the text.

$\tan\beta = 10$	$\mu = 111$ GeV	$M_1 = 1970$ GeV	$M_2 = 788$ GeV
$M_3 = 1399$ GeV	$A_t = 1000$ GeV	$A_b = 2800$ GeV	$A_\tau = 3000$ GeV
$m_{\chi_1^0} = 107.7$ GeV	$m_{\chi_1^\pm} = 111$ GeV	$m_{\tilde{e}_R} = 166$ GeV	$m_{\tilde{\nu}_e} = 136$ GeV
$m_{\chi_2^0} = 117$ GeV	$m_{\chi_2^\pm} = 806$ GeV	$m_{\tilde{e}_L} = 157$ GeV	$m_h = 125$ GeV

(1) $SO(10)$ where $SU(5)' \times U(1) \subset SO(10)$ with Φ and F_Φ in the **210**-dimensional representation with $SU(5)' \times U(1)$ in $(\mathbf{1}, \mathbf{0})$-dimensional representation (labelled as model $[SO(10)]_{210}$):

$$N_{1j} = (0.038, 0.194, -0.719, 0.666); \quad (3.5)$$

(2) $SO(10)$ where $SU(5)' \times U(1) \subset SO(10)$ with Φ and F_Φ in the **770**-dimensional representation with $SU(5)' \times U(1)$ in $(\mathbf{1}, \mathbf{0})$-dimensional representation (labelled as model $[SO(10)]_{770}$):

$$N_{1j} = (0.011, -0.193, 0.724, -0.663); \quad (3.6)$$

(3) $SO(10)$ where $SU(4) \times SU(2)_R \times SU(2)_L \subset SO(10)$ with Φ and F_Φ in the **770**-dimensional representation with $SU(4) \times SU(2)_R$ in $(\mathbf{1}, \mathbf{1})$-dimensional representation (labelled as model $[SO(10)]_{770'}$):

$$N_{1j} = (0.126, -0.660, 0.721, -0.678); \quad (3.7)$$

implying thereby that a Higgsino is the dominant component for the **210**- and **770**-dimensional representations with the embedding $SU(5)' \times U(1) \subset SO(10)$ and for the **770**-dimensional representation with the embedding $SU(4) \times SU(2)_R \times SU(2)_L \subset SO(10)$.

Thus, in these cases the dominant contribution to the radiative neutralino production cross section will come from the neutralino-Z^0 coupling. Since the LSP for most of the scenarios considered here has a dominant Higgsino component, the Z^0 width imposes a strict constraint, as the Z^0 decay rate involves coupling to the Higgsino component of the neutralino. We have imposed the LEP constraint on the anomalous Z^0 decay width in our calculations:

$$\Gamma(Z \to \tilde{\chi}_1^0 \tilde{\chi}_1^0) < 3 \text{ MeV}. \quad (3.8)$$

IV. RADIATIVE NEUTRALINO PRODUCTION IN GRAND UNIFIED THEORIES

In this section we calculate the cross section for the radiative neutralino production process,

$$e^-(p_1) + e^+(p_2) \to \tilde{\chi}_1^0(k_1) + \tilde{\chi}_1^0(k_2) + \gamma(q), \quad (4.1)$$

for the case of longitudinally polarized electron and positron beams for $SU(5)$ and $SO(10)$ grand unified theories with nonuniversal gaugino masses at the grand unified scale. The four-momenta of the corresponding particles are shown by the symbols in the brackets. We show in Fig. 1 the Feynman diagrams contributing to the radiative neutralino production at the tree level. The neutralino

TABLE V. Input parameters and resulting masses for various states in $SU(5)' \times U(1) \subset SO(10)$ supersymmetric grand unified theory with Φ and F_Φ in the **210**-dimensional representation with $SU(5)' \times U(1)$ in $(\mathbf{1}, \mathbf{0})$-dimensional representation. We shall refer to this model as $[SO(10)]_{210}$ in the text.

$\tan\beta = 10$	$\mu = 116$ GeV	$M_1 = -760$ GeV	$M_2 = 395$ GeV
$M_3 = 1405$ GeV	$A_t = 1000$ GeV	$A_b = 2800$ GeV	$A_\tau = 3000$ GeV
$m_{\chi_1^0} = 108$ GeV	$m_{\chi_1^\pm} = 111$ GeV	$m_{\tilde{e}_R} = 156$ GeV	$m_{\tilde{\nu}_e} = 136$ GeV
$m_{\chi_2^0} = 122$ GeV	$m_{\chi_2^\pm} = 421$ GeV	$m_{\tilde{e}_L} = 157$ GeV	$m_h = 126$ GeV

TABLE VI. Input parameters and resulting masses for various states in $SU(5)' \times U(1) \subset SO(10)$ supersymmetric grand unified theory with Φ and F_Φ in the **770**-dimensional representation with $SU(5)' \times U(1)$ in $(\mathbf{1}, \mathbf{0})$ dimensional representation. We shall refer to this model as $[SO(10)]_{770}$ in the text.

$\tan\beta = 10$	$\mu = 118$ GeV	$M_1 = 3038$ GeV	$M_2 = 395$ GeV
$M_3 = 1398$ GeV	$A_t = 1000$ GeV	$A_b = 2800$ GeV	$A_\tau = 3000$ GeV
$m_{\chi_1^0} = 108$ GeV	$m_{\chi_1^\pm} = 113$ GeV	$m_{\tilde{e}_R} = 156$ GeV	$m_{\tilde{\nu}_e} = 136$ GeV
$m_{\chi_2^0} = 126$ GeV	$m_{\chi_2^\pm} = 422$ GeV	$m_{\tilde{e}_L} = 157$ GeV	$m_h = 125.7$ GeV

TABLE VII. Input parameters and resulting masses for various states in $SU(4) \times SU(2)_R \times SU(2)_L \subset SO(10)$ supersymmetric grand unified theory with Φ and F_Φ in the **770**-dimensional representation with $SU(4) \times SU(2)_R$ in $(\mathbf{1}, \mathbf{1})$-dimensional representation. We shall refer to this model as $[SO(10)]_{770'}$ in the text.

$\tan\beta = 10$	$\mu = 113$ GeV	$M_1 = 378$ GeV	$M_2 = 985$ GeV
$M_3 = 1402$ GeV	$A_t = 1000$ GeV	$A_b = 2800$ GeV	$A_\tau = 3000$ GeV
$m_{\chi_1^0} = 108$ GeV	$m_{\chi_1^\pm} = 115$ GeV	$m_{\tilde{e}_R} = 156$ GeV	$m_{\tilde{\nu}_e} = 136$ GeV
$m_{\chi_2^0} = 121$ GeV	$m_{\chi_2^\pm} = 998$ GeV	$m_{\tilde{e}_L} = 157$ GeV	$m_h = 125$ GeV

mixing matrix (B2) summarized in Appendix B determines the couplings of the neutralinos to electrons, the selectrons, and to the Z^0 bosons. The respective values of the soft SUSY breaking gaugino mass parameters M_1 and M_2 for different grand unified models have been calculated in Appendix A. We further note that the elements of the neutralino mixing matrix N_{1j} for the different models considered here were calculated in the previous section.

A. Cross section for the signal process

At the tree level, the process (4.1) proceeds via the t- and u-channel exchange of right and left selectrons $\tilde{e}_{R,L}$ and via Z boson exchange in the s channel for the different scenarios considered here as can be seen from Fig. 1. The differential cross section for the process (4.1) can be written as [33,59]

$$d\sigma = \frac{1}{2} \frac{(2\pi)^4}{2s} \prod_f \frac{d^3\mathbf{p}_f}{(2\pi)^3 2E_f} \delta^{(4)}(p_1 + p_2 - k_1 - k_2 - q)|\mathcal{M}|^2,$$

(4.2)

where $\mathbf{p}_f$ and E_f are the final three-momenta $\mathbf{k}_1$, $\mathbf{k}_2$, $\mathbf{q}$ and the final energies E_{χ_1}, E_{χ_2}, and E_γ of the neutralinos and the photon, respectively. Using the standard technique, we sum over the spins of the neutralinos and the polarization of the outgoing photon. The squared matrix element $|\mathcal{M}|^2$ in Eq. (4.2) can then be written as [33]

$$|\mathcal{M}|^2 = \sum_{i \leq j} T_{ij},$$

(4.3)

where T_{ij} are squared amplitudes corresponding to the Feynman diagrams in Fig. 1. The phase space for the

radiative neutralino production process in Eq. (4.2) is described in detail in Ref. [33].

B. Longitudinal beam polarization

At the future linear collider, the use of beam polarization will significantly benefit the physics program. In the case of many processes, it is found that a suitable choice of beam polarizations can enhance the signal and suppress the background. At the ILC, a beam polarization of $\geq 80\%$ for electrons and $\geq 30\%$ for positrons at the interaction point is proposed, with a possible upgrading to about 60% for the positron beam. In the case of an electron and positron beam with arbitrary degree of longitudinal beam polarization, the total cross section in the center-of-mass frame with center-of-mass energy $\sqrt{s}$ is given by

$$\sigma_{P_{e^-} P_{e^+}} = \frac{1}{4}[(1 + P_{e^-})(1 - P_{e^+})\sigma_{RL}$$
$$+ (1 - P_{e^-})(1 + P_{e^+})\sigma_{LR}].$$

(4.4)

In Eq. (4.4) the dependence of the cross section on the polarization is parametrized through the degree of polarization, which is defined as $P_{e^\mp} = (N_R - N_L)/(N_R + N_L)$, where $N_{L,R}$ denote the number of left-polarized and right-polarized electrons (or positrons), respectively. Moreover σ_{RL} denotes the cross section when the electron beam is completely right polarized with $P_{e^-} = 1$ and the positron beam is completely left polarized with $P_{e^+} = -1$. An analogous definition holds for σ_{LR}. We do not take into account the helicity combinations for the cross section (LL and RR) as they are absent in the SM and for the supersymmetric process considered here. For the signal process, the significant contribution comes from the selectron or Z
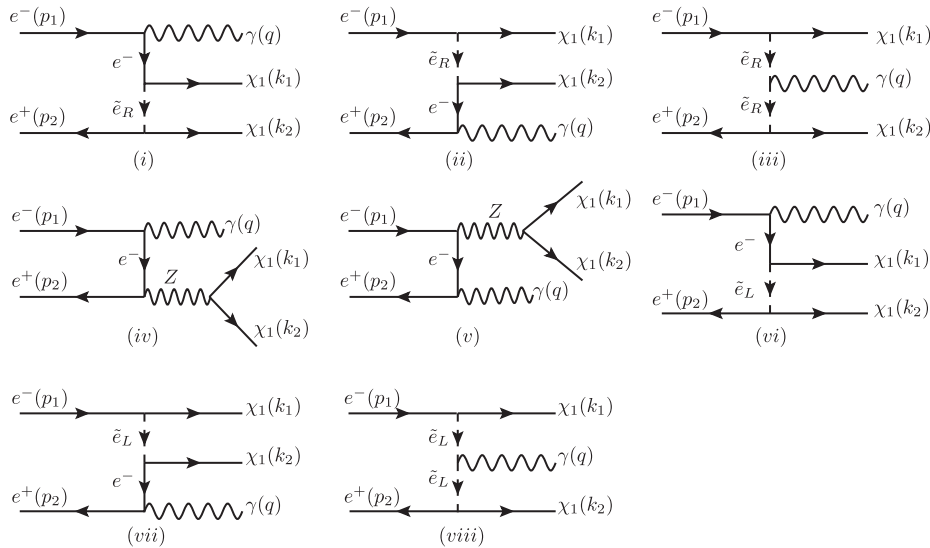

FIG. 1. Feynman diagrams contributing to the radiative neutralino production $e^+e^- \rightarrow \tilde{\chi}_1^0 \tilde{\chi}_1^0 \gamma$. There are six other diagrams which are exchange diagrams corresponding to (i, ii, iii, vi, vii, $viii$), with u-channel exchange of selectrons, wherein the neutralinos are crossed in the final state.

exchange depending on the composition of the neutralino. For all the scenarios considered, the neutralino is dominantly a Higgsino with the Z boson exchange dominantly contributing to the neutralino production process. In the case of $SU(5)_{24}$, the neutralino has a significant bino component resulting in significantly larger coupling to right selectron; therefore, the production process proceeds mainly via the exchange of right selectron $\tilde{e}_R$. On the other hand, the SM background radiative neutrino process proceeds mainly through the exchange of W bosons, which couple only to left-handed particles. Therefore, a polarization combination with positive electron beam polarization and negative positron beam polarization will significantly reduce the background and increase the signal for the cases where the neutralino has a dominant bino component. When the neutralino is of a Higgsino type, there is no appreciable change in cross section for this choice of beam polarization as Z couples to both left- and right-handed fermions. Since with this particular choice of beam polarization the SM background decreases, we present our result for this case with electron beam polarization $P_{e^-} = 0.8$ and positron beam polarization $P_{e^+} = -0.6$, as planned for the future linear collider.

C. Radiative corrections

The future high-energy e^+e^- colliders, in order to avoid energy losses from synchrotron radiation, are designed as linear colliders. These colliders will achieve high luminosity through beams with bunches of high number densities. Although the high density of charged particles increases the machine luminosity, it also leads to the generation of a strong electromagnetic field in and around every colliding bunch. Initial state radiation (ISR), also known as bremsstrahlung, which results from the interaction of the beam constituents with the accelerating field, is the most important QED correction to the Born cross section. Along with it, the interaction of the beam constituents due to the strong magnetic field generated by the other beam also results in radiation and is known as the beamstrahlung phenomenon. The general feature of both these cases results in multiple emissions of photons, both soft and hard, which not only reduces the initial beam energy but also results in the disturbance of the initial beam calibration. Moreover, at higher energies these radiative effects result in messier backgrounds with the radiated photons leading to the production of lepton pairs and hadrons. The resulting spectrum of the electrons due to the ISR effects mainly depends on the electron or positron beam energy and the reduced momentum of the incoming electron or positron. The photon radiation takes into account the missing momentum. On the other hand, the resulting spectrum due to beamstrahlung, apart from depending on the beam energy, is mainly machine specific depending on the number of electrons and positrons in a bunch N_e, the transverse bunch sizes σ_x, σ_y and the bunch length σ_z. Therefore, most future machine

TABLE VIII. Beam parameters for the ILC, where N is the number of particles in the bunch and σ_x, σ_y are the transverse bunch sizes at the interaction point, with σ_z as the bunch length.

Collider parameters	ILC
σ_x (nm)	640
σ_y (nm)	5.7
σ_z (μm)	300
N (10^{10})	2

designs try to minimize the radiation effects by adjusting the parameters of the bunches accordingly.

Apart from being a serious problem, the radiated photons have also been used in the study of new physics. The majority of the emitted photons are soft and are lost down the beam pipe. Only the hard photons with large transverse momentum can be tagged, and earlier they were used by the LEP experiments to look for the invisible final states. The most famous example is the neutrino counting process $e^+e^- \rightarrow \gamma \nu_l \bar{\nu}_l$ in the standard model, with the final state being a single photon and large missing energy. This search with a hard photon tag is similar to the supersymmetric process considered here in our work. In the case of LEP running at energies beyond the Z resonance, these radiative effects lead to "return of the Z peak" causing a hugely increased cross section. This was mainly due to the multiple emissions of photons resulting in the electron positron pair returning to the Z resonance. Therefore, taking into account all the above facts, the effect of the radiative effects, both ISR and beamstrahlung, is crucial for most experimental analyses.

Several strategies exist to include the radiative corrections in the calculations which have been studied exclusively in the past [60–63] in the context of the future linear colliders. We have calculated the radiative effects for our process and the background processes using CalcHEP [58], with parameters given in Table VIII [64]. In CalcHEP the energy spectrum of the electron and positron is calculated by using the structure function formalism. The main idea here is to include the radiative corrections by a probability density to find an electron with reduced momentum inside an incoming electron. This is quite similar to the techniques adopted for the hadronic interactions. The total cross section is defined as the leading-order cross section convoluted with the structure functions including radiative effects. These structure functions of the initial leptons are valid up to all orders in perturbation theory. We emphasize that in this paper the radiative effects are included in all our calculations of the signal and background processes.

V. NUMERICAL RESULTS

We have calculated the tree-level cross section for radiative neutralino production (4.1), the standard model background from radiative neutrino production (1.2), and

the supersymmetric background from sneutrino production (1.3) with longitudinally polarized electron and positron beams using the program CalcHEP [58]. As noted above we have included the effects of radiative corrections to the signal as well as the background processes. Due to the emission of soft photons, the tree-level cross sections have infrared and collinear divergences. These divergences are regularized by imposing cuts on the fraction of beam energy carried by the photon and the scattering angle of the photon [33]. We define the fraction of the beam energy carried by the photon as $x = E_\gamma / E_{\text{beam}}$, where $\sqrt{s} = 2E_{\text{beam}}$ is the center-of-mass energy, and E_γ is the energy carried away by the photon. The following cuts are then imposed on x and on the scattering angle θ_γ of the photon [65]:

$$0.02 \leq x \leq 1 - \frac{m^2_{\tilde{\chi}^0_1}}{E^2_{\text{beam}}}, \tag{5.1}$$

$$-0.95 \leq \cos\theta_\gamma \leq 0.95. \tag{5.2}$$

The lower and upper cut, Eq. (5.1), on the energy of the photon is a function of the beam energy. Interpreted in a different way, the upper cut corresponds to the kinematical limit of the radiative neutralino production process. In order to enhance the signal over the main SM background, with the neutrinos preferably emitted in the forward direction, the required detector acceptance cut, Eq. (5.2), on the photon is applied. Except for the cuts on energy and the angular spread, no other cut is found to significantly reduce the background. Therefore, we have implemented these cuts for both signal and background processes in the case of all the scenarios which we have considered in this work.

A. Photon energy (E_γ) distribution and total beam energy ($\sqrt{s}$) dependence

First of all we have calculated the energy distribution of the photons from the radiative neutralino production in case of the MSSM EWSB and different GUT scenarios with nonuniversal gaugino mass in the case of longitudinal beam polarization.

The energy distribution of the radiated photon in the presence of longitudinally polarized beams is shown in Figs. 2 and 3 for the scenarios with nonuniversal gaugino masses in grand unified theories based on $SU(5)$ and $SO(10)$. In these figures the resulting distributions are also compared with the MSSM EWSB model with universal gaugino masses at the GUT scale. Similarly the energy dependence of the total cross section is also calculated with the initially polarized beams and is shown in Figs. 4 and 5. Note that we have included radiative corrections in all these calculations. As discussed before we have restricted ourselves to only right-handed electron beams and left-handed positron beams in order to reduce the background. The degree of polarization used in our calculation is $(P_{e^-}, P_{e^+}) = (0.8, -0.6)$. The unpolarized case in case of
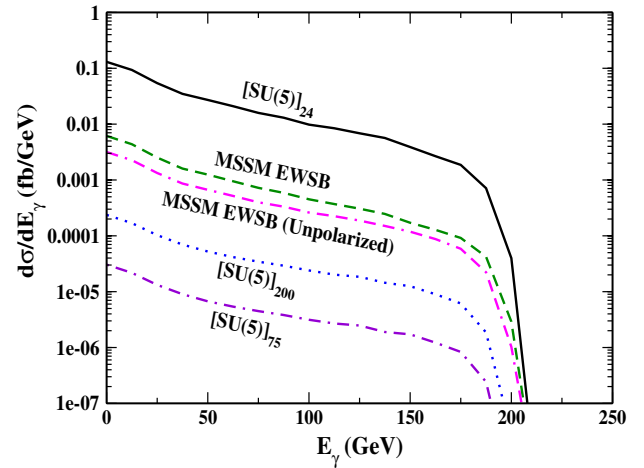

FIG. 2 (color online). The photon energy distribution $d\sigma/dE_\gamma$ for the radiative neutralino production including radiative effects with $(P_{e^-}, P_{e^+}) = (0.8, -0.6)$ in the case of $SU(5)$ with nonuniversal gaugino masses and in the case of the MSSM EWSB with universal gaugino masses. For comparison we have also shown the case of the MSSM EWSB with unpolarized beams.

the MSSM EWSB is also shown in these figures for the sake of comparison.

The signal in the case of MSSM EWSB and $[SU(5)]_{24}$ is enhanced in the polarized case compared to the other models considered here. The dominant component of the neutralino in $[SU(5)]_{24}$ is a bino, whereas in other cases the lightest neutralino is dominantly a Higgsino state. The MSSM EWSB scenario predicts a lightest neutralino with a dominant Higgsino component, but it also has a significant bino component leading to the enhancement of right selectron-electron-neutralino coupling. Therefore,
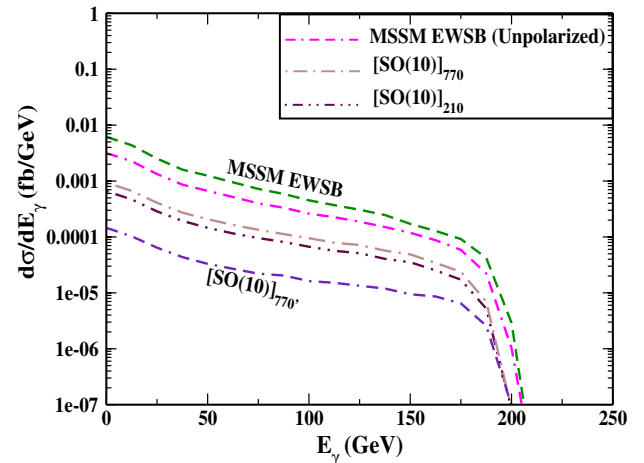

FIG. 3 (color online). The photon energy distribution $d\sigma/dE_\gamma$ including radiative effects for the radiative neutralino production with $(P_{e^-}, P_{e^+}) = (0.8, -0.6)$ in the case of $SO(10)$ with nonuniversal gaugino masses and in the case of the MSSM EWSB with universal gaugino masses. For comparison we have also shown the case of MSSM EWSB with unpolarized beams.
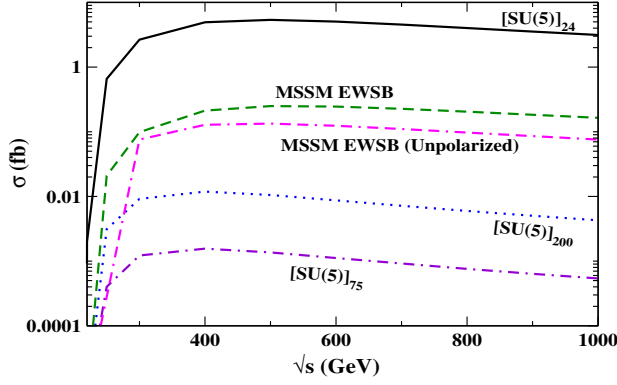
FIG. 4 (color online). Total cross section σ for the signal process, with the inclusion of radiative effects as a function of $\sqrt{s}$ with $(P_{e^-}, P_{e^+}) = (0.8, -0.6)$ for $SU(5)$ with nonuniversal gaugino masses and for the MSSM EWSB scenario with universal gaugino masses at the grand unified scale. For comparison we have also shown the case of MSSM EWSB with unpolarized beams.

FIG. 5 (color online). Total cross section σ for the signal process, with the inclusion of radiative effects as a function of $\sqrt{s}$ with $(P_{e^-}, P_{e^+}) = (0.8, -0.6)$ for $SO(10)$ with nonuniversal gaugino masses and for the MSSM EWSB scenario with universal gaugino masses at the grand unified scale. For comparison we have also shown the case of MSSM EWSB with unpolarized beams.
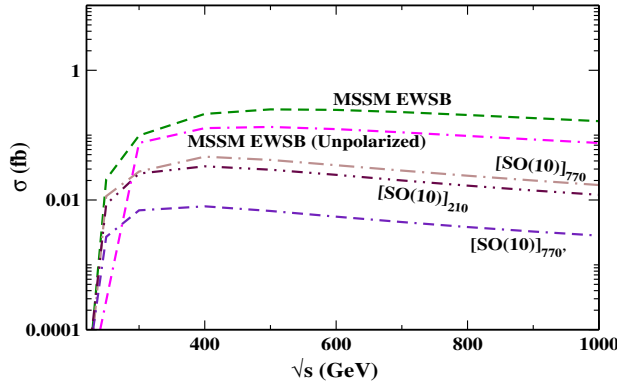
the choice of this particular polarization leads to an increase in the production cross section. For the other cases with a Higgsino-like neutralino, the t- and u- channel exchange of $\tilde{e}_{R,L}$ is suppressed, with the only contribution coming from off-shell Z decay. The Z boson due to its ability to combine with both left- and right-handed fermions does not result in significant changes with the inclusion of the beam polarization.

B. Dependence on μ and M_2

Since the mass of the lightest neutralino depends on the parameters μ and M_2, it is important to study the dependence of cross section for the signal process on these parameters. The dependence of the signal cross section is considered independently on the parameters μ and M_2.
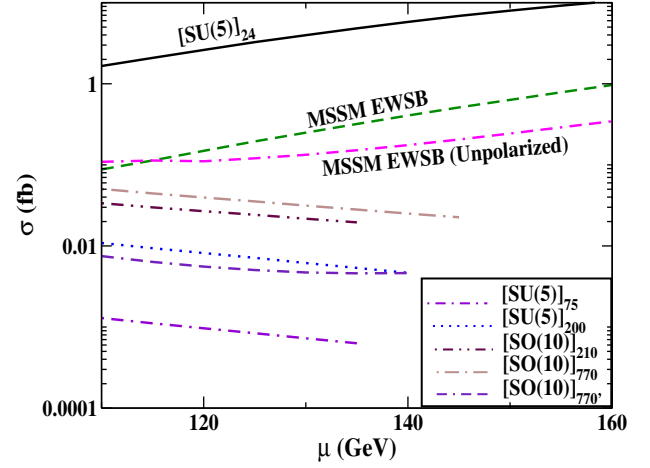

FIG. 6 (color online). The total radiative neutralino production cross section σ with radiative effects included as a function of μ in the range $\mu \, \epsilon \, [110, 160]$ GeV for different models at $\sqrt{s} = 500$ GeV with $(P_{e^-}, P_{e^+}) = (0.8, -0.6)$. For comparison we have also shown the case of MSSM EWSB with unpolarized beams.

The values of the parameters μ and M_2 are chosen in order to avoid color and charge breaking minima, unbounded from below constraint on scalar potential, and also to satisfy phenomenological constraints on different sparticle masses as discussed in Sec. II.

We have carried out a check on the parameter space used in our calculations on whether the complete scalar potential has charge and color breaking minima, which are lower than the electroweak symmetry breaking minimum. The condition of whether the scalar potential is unbounded from below has also been checked by us. The criteria used for these conditions are

$$A_f^2 < 3(m_{\tilde{f}_L}^2 + m_{\tilde{f}_R}^2 + \mu^2 + m_{H_2}), \tag{5.3}$$

$$m_{H_2} + m_{H_1} \geq 2|B\mu|, \tag{5.4}$$

respectively, at a scale $Q^2 > M_{\text{EWSB}}^2$. Here f denotes the fermion generation, and A is the trilinear supersymmetry breaking parameter. We have implemented these conditions through the SuSpect package [66], which computes the masses and couplings of the supersymmetric partners of the SM particles. For each model considered in this paper, we perform the renormalization group evolution to calculate the particle spectrum. While doing so we check for the consistency of the chosen parameter set with electroweak symmetry breaking and also whether the conditions (5.3) and (5.4) are satisfied.

In Fig. 6 we show the μ dependence of the cross section for different models considered in this paper for the polarized case along with the unpolarized case of MSSM EWSB. The cross section in the case of $SU(5)_{24}$ and MSSM EWSB is significantly enhanced compared to the unpolarized case. For the other scenarios, the behavior in
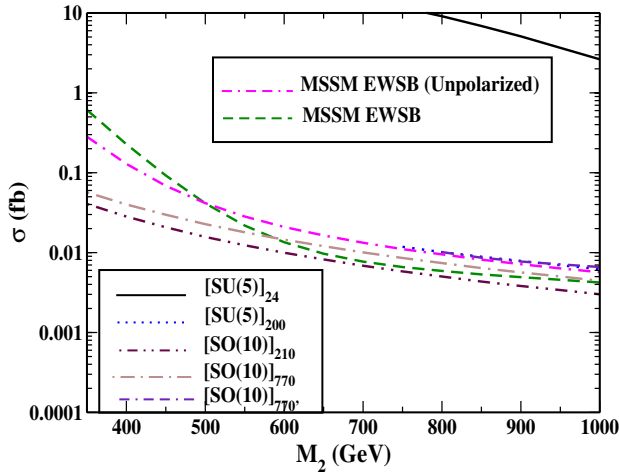
FIG. 7 (color online). Total cross section σ with the inclusion of radiative effects for the radiative neutralino production as a function of M_2 for different models with $M_2 \epsilon [390, 1000]$ GeV at $\sqrt{s} = 500$ GeV and $(P_{e^-}, P_{e^+}) = (0.8, -0.6)$. For comparison we have also shown the case of MSSM EWSB with unpolarized beams.

FIG. 8 (color online). Total cross section σ for the radiative neutralino production with radiative effects included vs $m_{\tilde{e}_L}$ at $\sqrt{s} = 500$ GeV with $(P_{e^-}, P_{e^+}) = (0.8, -0.6)$. For comparison we have also shown the case of MSSM EWSB with unpolarized beams.

the case of polarized beams is almost similar to the unpolarized case. It is found that for a wide range of μ, in the case of the $[SU(5)]_{24}$ and MSSM EWSB scenario, all the experimental constraints are satisfied, with $\tilde{\chi}_1^0$ as the LSP. For the other scenarios with a Higgsino-type lightest neutralino, the cross section is sensitive to the value of μ. Since $m_{\tilde{\chi}_1^0} \propto \mu$, above a certain value of μ, $\tilde{\chi}_1^0$ ceases to be the lightest supersymmetric particle. Depending on the percentage of the Higgsino component, the cross section changes with the value of μ. Most of the scenarios considered here are tightly constrained as a function of μ, with the neutralino as the LSP. This is due to the various limits on the sparticles masses from the experiments. The cross section for some scenarios in this region is too small to be observed at the ILC with $\sqrt{s} = 500$ GeV, even with an integrated luminosity of 500 fb^{-1}.

In Fig. 7 we show the dependence of the radiative neutralino cross section on the soft gaugino mass parameter M_2 for different models with polarized beams. In this case also $SU(5)_{24}$ and MSSM EWSB show an enhancement of the cross section, for smaller values of M_2. Since the total cross section decreases with increasing value of M_2, a lower value of M_2 favors a cross section which can be measured experimentally.

C. Dependence on selectron masses

The selectron masses are free parameters for the models considered here. Since the signal process proceeds mainly via right and left selectron $\tilde{e}_{R,L}$ exchange in the t and u channels, we have also considered the dependence of the total cross section on the selectron masses. The dependence on the selectron masses is shown in Figs. 8 and 9 in
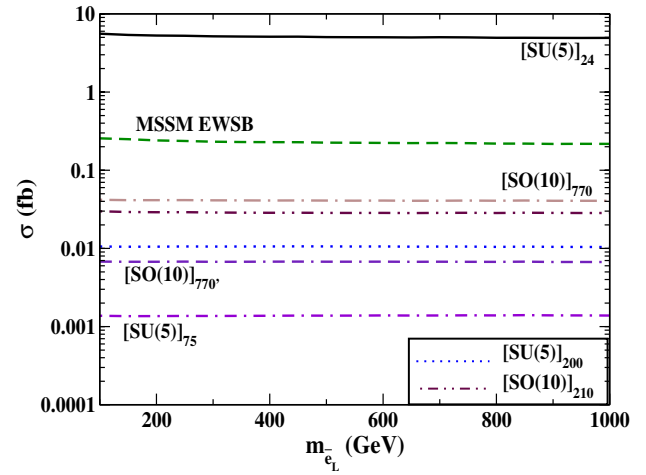

FIG. 9 (color online). Total cross section σ along with radiative effects for the radiative neutralino production vs $m_{\tilde{e}_R}$ at $\sqrt{s} = 500$ GeV with $(P_{e^-}, P_{e^+}) = (0.8, -0.6)$. For comparison we have also shown the case of MSSM EWSB with unpolarized beams.
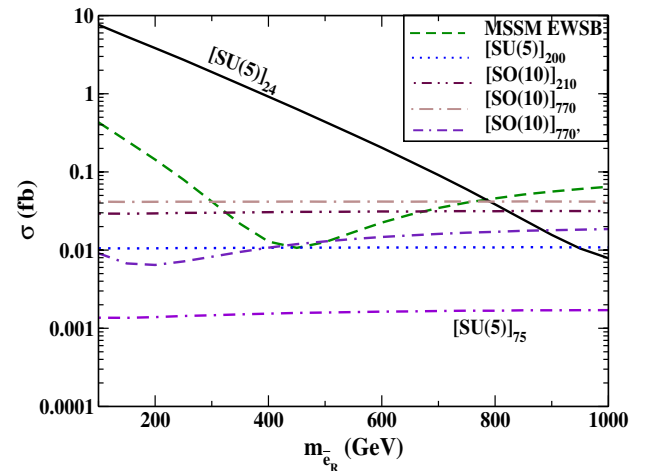
the case of polarized beams and for unpolarized beams in the case of MSSM EWSB. The cross section is insensitive to the left selectron mass in case of all models. For $SU(5)_{24}$, the neutralino being a bino, the cross section is sensitive to the right selectron mass and decreases with increasing $m_{\tilde{e}_R}$ and has a negligible sensitivity to left selectron mass. The MSSM EWSB shows a peculiar behavior with respect to the right selectron mass. This is mainly because the neutralino in this case has a dominant Higgsino component along with a significant bino component. Therefore, the signal process in this scenario receives contribution from both the right selectron exchange
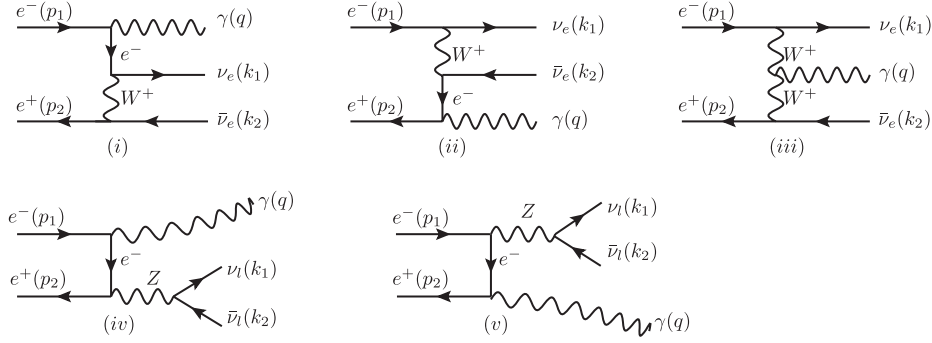
FIG. 10. Feynman diagrams contributing to the radiative neutrino process $e^+ e^- \rightarrow \nu \bar{\nu} \gamma$ where (*iv* and *v*) corresponds to the neutrinos of three flavors.

channel and the Z exchange channel. This behavior arises due to the interference term from these two diagrams and is sensitive to the center-of-mass energy. Note that for this particular choice of beam polarization, this behavior is more enhanced as one of the contributing diagrams is due to $\tilde{e}_R$ exchange. If the beam polarization would have been due to left-handed electrons and right-handed positrons, there would be no contribution from the right selectron exchange diagram. Therefore, the cross section in that case will be insensitive to $m_{\tilde{e}_R}$. The other models have a Higgsino-type neutralino; therefore, their production cross section shows no dependence on the selectron masses.

VI. BACKGROUND PROCESSES

A. Neutrino background

For the signal process (4.1) considered here, the main background comes from the SM radiative neutrino production. The other possible backgrounds are from $e^+ e^- \rightarrow \tau^+ \tau^- \gamma$, with both the τ's decaying to soft leptons or hadrons, but the contribution from this process is found to be negligible. Another large background comes from the radiative Bhabha scattering, $e^+ e^- \rightarrow e^+ e^- \gamma$, where $e^{\pm'}$s are not detected. This radiative scattering is usually eliminated by imposing a cut on E_γ. The events are selected by imposing the condition that any particle other than γ appearing in the angular range $-0.95 < \cos \theta_\gamma < 0.95$ must have energy less than $E_{\max}$, where $E_{\max}$ is detector dependent, but presumably no larger than a few GeV. This is discussed in detail in the literature [67].

The SM radiative neutrino production

$$ e^+ + e^- \rightarrow \nu_\ell + \bar{\nu}_\ell + \gamma, \qquad \ell = e, \mu, \tau \qquad (6.1) $$

has been studied extensively [40,48,68–70]. For this background process, ν_e are produced via t-channel W boson exchange and $\nu_{e,\mu,\tau}$ via s-channel Z boson exchange. The corresponding Feynman diagrams are shown in Fig. 10.

Since the photons emitted from this process mostly tend to be collinear, therefore the angular cut on the photon is applied to separate it from the signal photons. This process mainly proceeds through the exchange of W boson which

couples only to the left-handed fermions. We are considering the case of beam polarization with right-handed electron and left-handed positron. The respective degree of polarization is $P_{e^-} = 0.8$ and $P_{e^+} = -0.6$. Figure 11 shows that the photon energy distribution from the radiative neutrino production, whereas in Fig. 12 we show the $\sqrt{s}$ dependence of the total radiative neutrino cross section. Note that the radiative corrections are included here. The unpolarized case is also shown in the figures for comparison. It is observed that with this choice of beam polarization, the W bosons in the intermediate state do not contribute, and the cross section is significantly reduced. For instance, at $\sqrt{s} = 500$ GeV with the inclusion of radiative corrections and the cuts, the total unpolarized cross section σ_{unpol} is 2432 fb, whereas with the inclusion of this particular beam polarization, σ_{pol} is 398 fb. The background is reduced by 1 order of magnitude. Due to the production of Z boson through the s channel the photon energy distribution peaks for $E_\gamma = (s - 4m_Z^2)/(2\sqrt{s}) \approx 218$ GeV at $\sqrt{s} = 500$ GeV. By imposing an upper cut
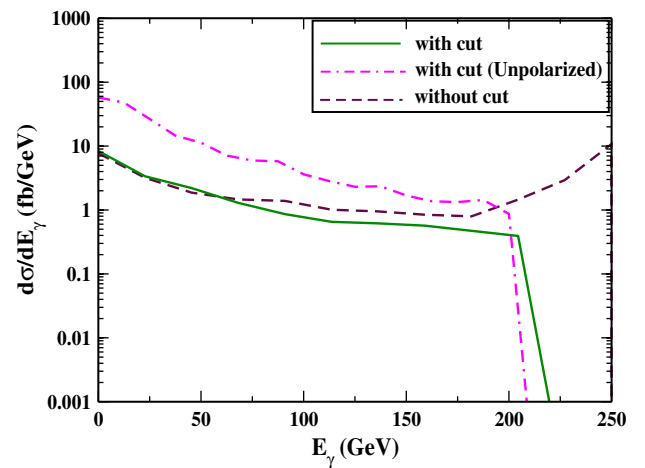

FIG. 11 (color online). Plot showing the photon energy distribution $d\sigma/dE_\gamma$ for the radiative neutrino production process $e^+ e^- \rightarrow \nu \bar{\nu} \gamma$ at $\sqrt{s} = 500$ GeV, with the inclusion of radiative effects and $(P_{e^-}, P_{e^+}) = (0.8, -0.6)$.
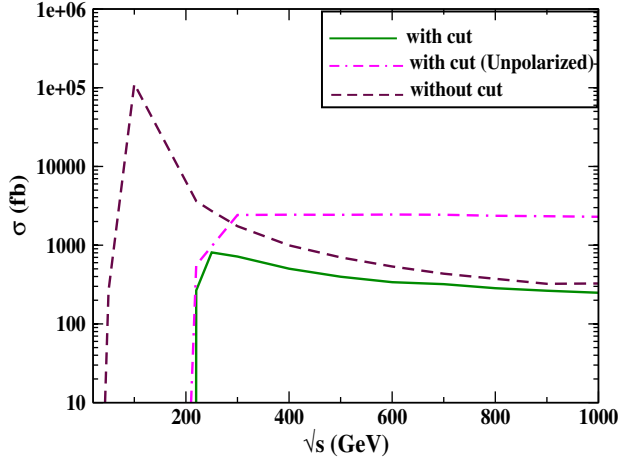
FIG. 12 (color online).   The total energy $\sqrt{s}$ dependence of the radiative neutrino cross section with and without an upper cut on the photon energy E_γ, along with the radiative effects and $(P_{e^-}, P_{e^+}) = (0.8, -0.6)$.

on the photon energy, which depends on the neutralino mass, see Eq. (5.1), the photon background from radiative neutrino production is reduced. A similar argument holds for the production cross section where the on-shell Z produced through this background process is eliminated by imposing an upper cut on the photon energy.

B. Supersymmetric background

Apart from the SM background, the signal process (4.1) under consideration has also a supersymmetric background from the sneutrino production process [40,71]:

$$e^+ + e^- \to \tilde{\nu}_\ell + \tilde{\nu}_\ell^* + \gamma, \qquad \ell = e, \mu, \tau. \quad (6.2)$$

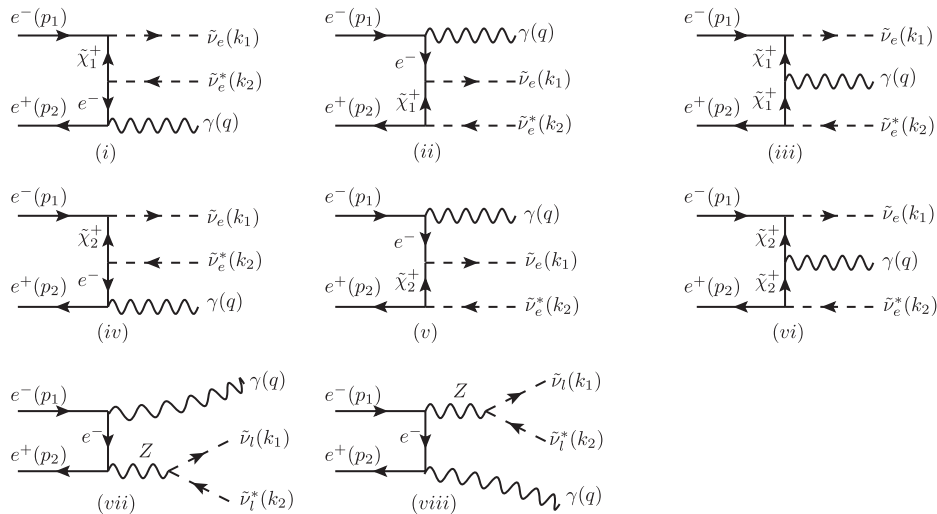In Fig. 13 we show the tree-level Feynman diagrams contributing to the supersymmetric background process

under study. Apart from the s-channel contribution from Z boson, the process also receives a t-channel contribution from the virtual charginos. Due to the contribution from virtual charginos, this process is sensitive to the chargino mixing matrix **U**. In Fig. 14 we show the photon energy distribution for the supersymmetric background process at $\sqrt{s} = 500$ GeV for the different models, whereas the total production cross section is shown in Fig. 15. We have applied the same cuts for this process as in the signal process and have used an initial beam polarization of $P_{e^-} = 0.8$, $P_{e^+} = -0.6$. Similar to the radiative neutrino and neutralino production, the unpolarized case of MSSM EWSB is also included in the figures. The process is not sensitive to initial beam polarization, with the cross section and the photon energy distribution in the case of polarized beams behaving almost similarly to the unpolarized case. From Figs. 14 and 15, it is seen that for $[SU(5)]_{24}$, $[SU(5)]_{75}$, $[SU(5)]_{200}$ and $[SO(10)]_{770'}$, the behavior of the cross section is similar. This is due to the mixing matrix **U** being same for all the models considered here.

This process can act as a major supersymmetric background to the signal if the sneutrinos decay invisibly via $\tilde{\nu} \to \tilde{\chi}_1^0 \nu$. This scenario has been called the "virtual LSP" scenario [40]. But the sneutrinos can decay to other particles if kinematically allowed, thus reducing its contribution to the signal. We note that the other prominent decay channels are $\tilde{\nu} \to \tilde{\chi}_1^\pm \ell^\mp$ and $\tilde{\nu} \to \tilde{\chi}_2^0 \nu$, if kinematically allowed. For the scenarios with a bino-type neutralino, the dominant decay mode is the invisible decay channel with 100% branching ratio. For the scenarios with a Higgsino-type neutralino, the various decay channels are presented in Table IX.

There can also be other supersymmetric background from the neutralino production $e^+ e^- \to \tilde{\chi}_1^0 \tilde{\chi}_2^0$, with the subsequent radiative decay [72] of the next-to-lightest neutralino $\tilde{\chi}_2^0 \to \tilde{\chi}_1^0 \gamma$. The branching ratios for this decay

FIG. 13.   Feynman diagrams contributing to the radiative sneutrino production process $e^+ e^- \to \tilde{\nu}\tilde{\nu}^*\gamma$, with the last two diagrams (*vii* and *viii*) corresponding to all the leptonic sneutrino.
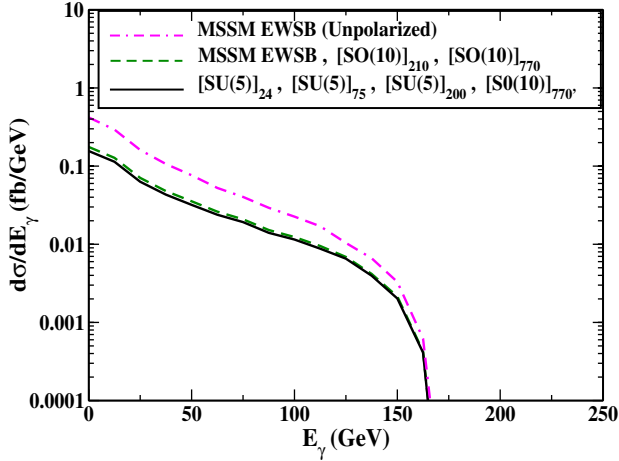
FIG. 14 (color online). Plot showing the photon energy distribution $d\sigma/dE_\gamma$ for the radiative sneutrino production process $e^+e^- \to \tilde{\nu}\tilde{\nu}^*\gamma$ at $\sqrt{s} = 500$ GeV, with the inclusion of radiative effects and initial beam polarization $(P_{e^-}, P_{e^+}) = (0.8, -0.6)$. For comparison we have also shown the case of MSSM EWSB with unpolarized beams.

FIG. 15 (color online). The total energy $\sqrt{s}$ dependence of the radiative sneutrino cross section $e^+e^- \to \tilde{\nu}\tilde{\nu}^*\gamma$ with an upper cut on the photon energy E_γ and the inclusion of radiative effects and initial beam polarization $(P_{e^-}, P_{e^+}) = (0.8, -0.6)$. For comparison we have also shown the case of MSSM EWSB with unpolarized beams.

are too small, with a significant ratio obtained for small values of $\tan\beta < 5$ or $M_1 \sim M_2$ [41,73,74]. Therefore, we have neglected this process in our study; however, a detailed discussion of this process can be found in Refs. [73–75].

C. Theoretical significance

Finally we discuss whether the photons from the signal process can be measured over the photons from the background. This is expressed in terms of theoretical significance for a given integrated luminosity $\mathcal{L}$ and is defined as [65]

$$S = \frac{N_S}{\sqrt{N_S + N_B}} = \frac{\sigma}{\sqrt{\sigma + \sigma_B}}\sqrt{\mathcal{L}}. \quad (6.3)$$

In the above equation $N_S = \sigma\mathcal{L}$ is the number of signal photons, and $N_B = \sigma_B\mathcal{L}$ denotes the number of background photons. For the detection of a signal, a theoretical significance of 5 is required, whereas the signal can be measured at a 68% confidence level for a theoretical significance of $S = 1$. In Fig. 16 we show the μ dependence of the theoretical significance S for the different models considered here for an initial beam polarization of $P_{e^-} = 0.8$ and $P_{e^+} = -0.6$. When the lightest
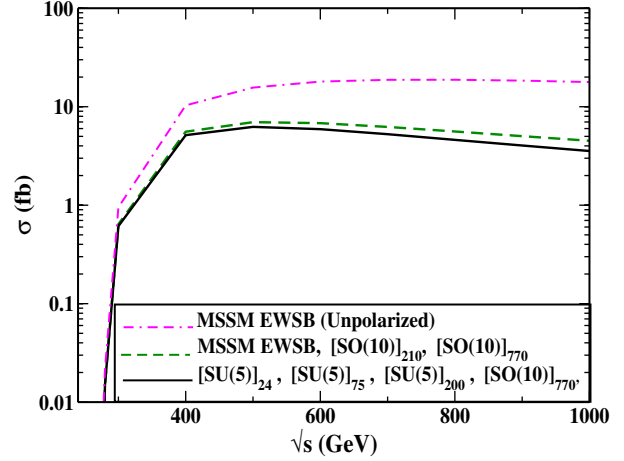
neutralino is dominantly a bino as in the case of $[SU(5)]_{24}$, or a has dominant bino and Higgsino components, as in the case of MSSM EWSB, the choice of this beam polarization significantly enhances the signal compared to the unpolarized case. In the case of unpolarized beams, S for the considered μ range has a maximum value of 2 in the case of $[SU(5)]_{24}$, whereas for this choice of beam polarization, it has a maximum value of 12. Similar behavior follows in case of MSSM EWSB. It can be seen from the Fig. 16 that it will be difficult to observe the signal for the other scenarios considered here with the lightest neutralino having a dominant Higgsino component.

We have also studied the variation of theoretical significance S as a function of the gaugino mass parameter M_2. In Fig. 17 we show the M_2 dependence of S for all the models considered in this work in the interval $M_2 \epsilon [200, 1000]$ GeV. A behavior almost similar to the μ dependence of S is observed.

Along with S we have also considered the signal-to-background ratio defined as

$$r = \frac{\sigma}{\sigma_B}. \quad (6.4)$$

The values of S and r can serve as a good guideline for our analysis since we do not consider detector simulation

TABLE IX. Branching ratios of the sneutrino for different models with a Higgsino-type lightest neutralino.

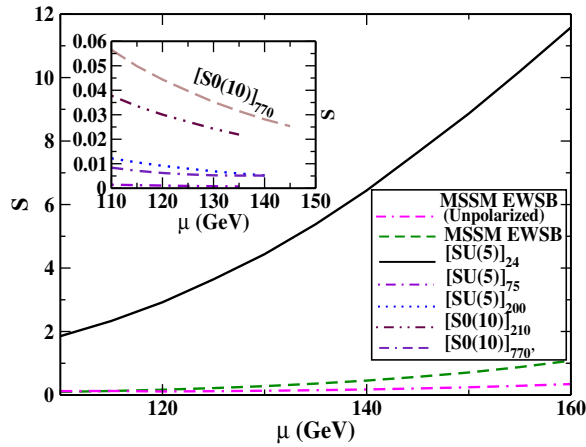| Branching ratios	MSSM EWSB	$SU(5)_{75}$	$SU(5)_{200}$	$SO(10)_{210}$	$SO(10)_{770}$	$SO(10)_{770'}$
$BR(\tilde{\nu}_e \to \tilde{\chi}_1^0 \nu_e)$	78.4%	8.1%	21.2%	18%	24.2%	44.4%
$BR(\tilde{\nu}_e \to \tilde{\chi}_2^0 \nu_e)$		1.8%	4.54%	0.8%	1.2%	6%
$BR(\tilde{\nu} \to \tilde{\chi}_1^\mp \ell^\pm)$	21.6%	90.1%	74.3%	81%	74.8%	49.6%

FIG. 16 (color online). Plot showing the theoretical significance S for the radiative neutralino production as a function of μ for different models considered in this paper with $\sqrt{s} = 500$ GeV and $(P_{e^-}, P_{e^+}) = (0.8, -0.6)$. For comparison we have also shown the case of MSSM EWSB with unpolarized beams.
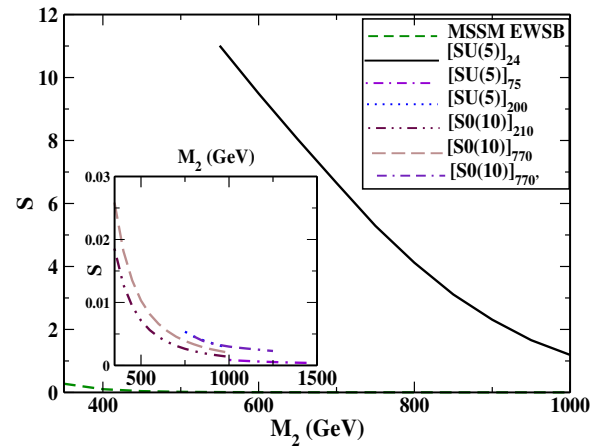

FIG. 17 (color online). The theoretical significance S for the radiative neutralino production as a function of the gaugino mass parameter M_2 for the different models with $\sqrt{s} = 500$ GeV and $(P_{e^-}, P_{e^+}) = (0.8, -0.6)$. The case of unpolarized beams for MSSM EWSB is not shown here as it coincides with the polarized case.

here, which is beyond the scope of the present paper. In the case of the ILC, for a signal to be detectable, r is required to be greater than 1%. Since the future collider is designed for planned energies of 500, 800, and 1000 GeV, we have presented the signal and background cross sections along with S and r for these energies and different cases of a longitudinally polarized beam for an integrated luminosity

of 500 fb^{-1}. We present the values of the total cross section, the significance, and the signal-to-background ratio for all the scenarios considered here for different center-of-mass energies in Tables X, XI, and XII. The set of parameters considered for the different models is listed in Tables I, II, III, IV, V, VI, and VII. It can be seen from Tables X, XI, and XII that there is an enhancement in S and

TABLE X. Signal and background cross sections σ, significance S, and signal-to-background ratio r in the case of different beam polarizations $(P_{e^-}|P_{e^+})$ for the different scenarios at $\sqrt{s} = 500$ GeV for $\mathcal{L} = 500$ fb^{-1}.

	$(P_{e^-}|P_{e^+})$	(0|0)	(0.8|0)	(0.8| − 0.3)	(0.8| − 0.6)	(0.9|0)	(0.9| − 0.3)	(0.9| − 0.6)
SM background	$\sigma(e^+e^- \to \nu\bar{\nu}\gamma)$ (fb)	2432	577	481	398	335	314	295
MSSM EWSB	$\sigma(e^+e^- \to \tilde{\chi}_1^0\tilde{\chi}_1^0\gamma)$ (fb)	0.1377	0.1651	0.2096	0.2495	0.1704	0.2172	0.2601
	S	0.0624	0.1536	0.2136	0.2795	0.2081	0.2739	0.3384
	r	0.0056	0.0286	0.0435	0.0626	0.0508	0.0691	0.0881
$[SU(5)]_{24}$	$\sigma(e^+e^- \to \tilde{\chi}_1^0\tilde{\chi}_1^0\gamma)$ (fb)	1.883	3.391	4.432	5.376	3.551	4.626	5.758
	S	0.8534	3.1470	4.4978	5.9850	4.3150	5.7947	7.4239
	r	0.0774	0.5876	0.9214	1.3507	1.0600	1.4732	1.9518
$[SU(5)]_{75}$	$\sigma(e^+e^- \to \tilde{\chi}_1^0\tilde{\chi}_1^0\gamma)$ (fb)	0.0007	0.0009	0.0011	0.0014	0.0009	0.0012	0.0014
	S	0.0003	0.0008	0.0011	0.0015	0.0010	0.0015	0.0018
	r	0.0000	0.0001	0.0002	0.0003	0.0002	0.0003	0.0004
$[SU(5)]_{200}$	$\sigma(e^+e^- \to \tilde{\chi}_1^0\tilde{\chi}_1^0\gamma)$ (fb)	0.0067	0.0071	0.0089	0.0105	0.0071	0.0091	0.0108
	S	0.0030	0.0066	0.0090	0.0117	0.0086	0.0114	0.0140
	r	0.0002	0.0012	0.0018	0.0026	0.0021	0.0028	0.0036
$[SO(10)]_{210}$	$\sigma(e^+e^- \to \tilde{\chi}_1^0\tilde{\chi}_1^0\gamma)$ (fb)	0.0150	0.0191	0.0244	0.0293	0.0195	0.0252	0.0310
	S	0.0068	0.0177	0.0248	0.0328	0.0238	0.0317	0.0403
	r	0.0006	0.0033	0.0050	0.0073	0.0058	0.0080	0.0105
$[SO(10)]_{770}$	$\sigma(e^+e^- \to \tilde{\chi}_1^0\tilde{\chi}_1^0\gamma)$ (fb)	0.0193	0.0267	0.0344	0.0415	0.0275	0.0357	0.0440
	S	0.0087	0.0248	0.0350	0.0465	0.0335	0.0450	0.0572
	r	0.0007	0.0047	0.0071	0.0104	0.0082	0.0136	0.0149
$[SO(10)]_{770'}$	$\sigma(e^+e^- \to \tilde{\chi}_1^0\tilde{\chi}_1^0\gamma)$ (fb)	0.0117	0.0055	0.0061	0.0066	0.0048	0.0056	0.0065
	S	0.0053	0.0051	0.0062	0.0073	0.0058	0.0070	0.0084
	r	0.0004	0.0009	0.0012	0.0016	0.0014	0.0017	0.0022

TABLE XI. Signal and background cross sections σ, significance S, and signal-to-background ratio r in the case of different beam polarizations $(P_{e^-}|P_{e^+})$ for the different scenarios at $\sqrt{s} = 800$ GeV for $\mathcal{L} = 500$ fb^{-1}.

	$(P_{e^-}|P_{e^+})$	$(0|0)$	$(0.8|0)$	$(0.8|-0.3)$	$(0.8|-0.6)$	$(0.9|0)$	$(0.9|-0.3)$	$(0.9|-0.6)$
SM background	$\sigma(e^+e^- \to \nu\bar{\nu}\gamma)$ (fb)	2365	505	375	284	280	230	177
MSSM EWSB	$\sigma(e^+e^- \to \tilde{\chi}_1^0\tilde{\chi}_1^0\gamma)$ (fb)	0.1002	0.1343	0.1690	0.2055	0.1371	0.1772	0.2168
	S	0.0460	0.1336	0.1950	0.2725	0.1831	0.2611	0.3641
	r	0.0042	0.0265	0.0450	0.0723	0.0489	0.0770	0.1224
$[SU(5)]_{24}$	$\sigma(e^+e^- \to \tilde{\chi}_1^0\tilde{\chi}_1^0\gamma)$ (fb)	1.4103	2.5440	3.3289	4.0442	2.6612	3.4729	4.3246
	S	0.6482	2.5249	3.8268	5.3280	3.5392	5.0821	7.1810
	r	0.0596	0.5037	0.8877	1.4240	0.9504	1.5100	2.4433
$[SU(5)]_{75}$	$\sigma(e^+e^- \to \tilde{\chi}_1^0\tilde{\chi}_1^0\gamma)$ (fb)	0.0004	0.0005	0.0006	0.0008	0.0005	0.0007	0.0008
	S	0.0001	0.0004	0.0006	0.0010	0.0006	0.0010	0.0013
	r	0.0000	0.0000	0.0001	0.0002	0.0001	0.0003	0.0004
$[SU(5)]_{200}$	$\sigma(e^+e^- \to \tilde{\chi}_1^0\tilde{\chi}_1^0\gamma)$ (fb)	0.0037	0.0040	0.0051	0.0060	0.0042	0.0052	0.0063
	S	0.0017	0.0039	0.0058	0.0079	0.0056	0.0076	0.0105
	r	0.0001	0.0007	0.0013	0.0021	0.0015	0.0022	0.0035
$[SO(10)]_{210}$	$\sigma(e^+e^- \to \tilde{\chi}_1^0\tilde{\chi}_1^0\gamma)$ (fb)	0.0097	0.0111	0.0140	0.0167	0.0112	0.0144	0.0176
	S	0.0044	0.0110	0.0161	0.0221	0.0149	0.0212	0.0295
	r	0.0004	0.0021	0.0037	0.0058	0.0040	0.0062	0.0099
$[SO(10)]_{770}$	$\sigma(e^+e^- \to \tilde{\chi}_1^0\tilde{\chi}_1^0\gamma)$ (fb)	0.0112	0.0154	0.0197	0.0238	0.0158	0.0205	0.0252
	S	0.0051	0.1532	0.0227	0.0315	0.0211	0.0302	0.0423
	r	0.0004	0.0304	0.0052	0.0083	0.0056	0.0089	0.0142
$[SO(10)]_{770'}$	$\sigma(e^+e^- \to \tilde{\chi}_1^0\tilde{\chi}_1^0\gamma)$ (fb)	0.0067	0.0032	0.0035	0.0038	0.0027	0.0033	0.0038
	S	0.0030	0.0031	0.0040	0.0050	0.0036	0.0048	0.0063
	r	0.0002	0.0006	0.0009	0.0013	0.0009	0.0014	0.0021

TABLE XII. Signal and background cross sections σ, significance S, and signal-to-background ratio r in the case of different beam polarizations $(P_{e^-}|P_{e^+})$ for the different scenarios at $\sqrt{s} = 1000$ GeV for $\mathcal{L} = 500$ fb^{-1}.

	$(P_{e^-}|P_{e^+})$	$(0|0)$	$(0.8|0)$	$(0.8|-0.3)$	$(0.8|-0.6)$	$(0.9|0)$	$(0.9|-0.3)$	$(0.9|-0.6)$
SM background	$\sigma(e^+e^- \to \nu\bar{\nu}\gamma)$ (fb)	2293	482	356	248	257	204	155
MSSM EWSB	$\sigma(e^+e^- \to \tilde{\chi}_1^0\tilde{\chi}_1^0\gamma)$ (fb)	0.0781	0.1073	0.1378	0.1652	0.1100	0.1431	0.1759
	S	0.0364	0.1092	5.8147	0.2344	0.1533	0.2239	0.3157
	r	0.0034	0.0222	0.0387	0.0666	0.0428	0.0701	0.1134
$[SU(5)]_{24}$	$\sigma(e^+e^- \to \tilde{\chi}_1^0\tilde{\chi}_1^0\gamma)$ (fb)	1.1022	1.9900	2.6008	3.1510	2.0845	2.7096	3.3768
	S	0.5145	2.0225	3.0709	4.4338	8.6425	4.2140	5.999
	r	0.0480	0.4128	0.7305	1.2705	0.8110	1.328	2.1786
$[SU(5)]_{75}$	$\sigma(e^+e^- \to \tilde{\chi}_1^0\tilde{\chi}_1^0\gamma)$ (fb)	0.0003	0.0004	0.0005	0.0005	0.0004	0.0005	0.0006
	S	0.0001	0.0004	0.0006	0.0007	0.0005	0.0007	0.0010
	r	0.0000	0.0000	0.0001	0.0002	0.0002	0.0003	0.0004
$[SU(5)]_{200}$	$\sigma(e^+e^- \to \tilde{\chi}_1^0\tilde{\chi}_1^0\gamma)$ (fb)	0.0027	0.0029	0.0036	0.0043	0.0029	0.0037	0.0045
	S	0.0012	0.0029	0.0042	0.0061	0.0040	0.0057	0.0080
	r	0.0001	0.0006	0.0010	0.0017	0.0011	0.0018	0.0029
$[SO(10)]_{210}$	$\sigma(e^+e^- \to \tilde{\chi}_1^0\tilde{\chi}_1^0\gamma)$ (fb)	0.0074	0.0081	0.0100	0.0121	0.0081	0.0104	0.0126
	S	0.0034	0.0082	0.0118	0.1561	0.0112	0.0162	0.0226
	r	0.0003	0.0017	0.0028	0.0017	0.0032	0.0051	0.0081
$[SO(10)]_{770}$	$\sigma(e^+e^- \to \tilde{\chi}_1^0\tilde{\chi}_1^0\gamma)$ (fb)	0.0082	0.0111	0.0142	0.0171	0.0114	0.0147	0.0181
	S	0.0038	0.0113	0.0168	0.0242	0.0159	0.0229	0.0325
	r	0.0004	0.0023	0.0040	0.0069	0.0044	0.0072	0.0116
$[SO(10)]_{770'}$	$\sigma(e^+e^- \to \tilde{\chi}_1^0\tilde{\chi}_1^0\gamma)$ (fb)	0.0048	0.0023	0.0026	0.0028	0.002	0.0024	0.0028
	S	0.0048	0.0023	0.0030	0.0039	0.0027	0.0037	0.0050
	r	0.0002	0.0005	0.0007	0.0011	0.0008	0.0012	0.0032

r when we move from the unpolarized to the polarized case. The enhancement is significant for the case of beam polarization $(0.9| - 0.6)$. The behavior is similar with the bino-type neutralino having a significant value of S and r, making the signal observable at the ILC for different cases of beam polarization. But for the scenarios with a Higgsino-type neutralino, the values of S and r are too small, making it difficult to test them at the future linear colliders through this radiative neutralino production process.

D. Left-right asymmetry

In this subsection, we consider as an observable the left-right asymmetry as a means to distinguish between various grand unified models. In order to obtain a better efficiency, we consider the integral version of this asymmetry. The integrated left-right asymmetry is defined as

$$A_{LR} = \frac{\sigma_{LR} - \sigma_{RL}}{\sigma_{LR} + \sigma_{RL}}, \qquad (6.5)$$

where σ_{RL} and σ_{LR} are defined in Sec. IV B. The coupling of the lightest neutralino to the selectron and a fermion is different for left- and right- handed fermions, with different couplings, for the different models that we have considered in this paper. The coupling is relatively sensitive to the composition of the lightest neutralino, and one would expect an appreciable difference between the left- and right-polarized cross section. It can be seen from Table XVII that the lightest neutralino with a dominant wino and bino composition is sensitive to beam polarization, whereas the Higgsino-type neutralino has no dependence on beam We plot in Fig. 18 the left-right asymmetry for the different models for the radiative neutralino production as a function of the center-of-mass energy. The SM background (radiative neutrino production) is also considered here. The dependence of the various models on beam

FIG. 18 (color online). Plot showing the left-right asymmetry as a function of the center-of-mass energy for radiative neutralino production in the case of different models along with the SM background from radiative neutrino production.

polarization can be easily understood from Fig. 18. In the case of radiative neutrino production, as discussed before, since the cross section gets highly suppressed with positive electron and negative positron beam polarization, A_{LR} in this case is the largest. A_{LR} is also larger for the models where the lightest neutralino is mainly a bino or a wino, i.e., enhanced couplings to the selectrons. Since $SU(5)_{24}$, $SO(10)_{770'}$ have a bino- and wino-type lightest neutralino, A_{LR}, in this case is close to 1 or greater than 0.5. But for most of the models ($SU(5)_{75}$, $SU(5)_{200}$, $SO(10)_{210}$, $SO(10)_{770}$, $SO(10)_{770'}$), A_{LR} is less than 0.5 since they have the lightest neutralino with a dominant Higgsino component, with practically no beam polarization dependence from the exchange of selectrons. The result is almost independent of the center-of-mass energy.

VII. SUMMARY AND CONCLUSIONS

In this paper we have carried out a detailed study of the radiative neutralino production $e^+e^- \rightarrow \tilde{\chi}_1^0 \tilde{\chi}_1^0 \gamma$ for the case of $SU(5)$ and $SO(10)$ supersymmetric GUT models for ILC energies with longitudinally polarized e^- and e^+ beams. In these GUT models, the boundary conditions on the soft gaugino mass parameters can be nonuniversal. We have compared the results of these GUT models with the corresponding results in the MSSM with universal gaugino mass parameters (universal boundary conditions). For our analyses we have used a particular set of parameter values for various models by imposing theoretical and experimental constraints as discussed in Sec. II. The radiative neutralino production process has a signature of a high-energy photon and missing energy. The background to the signal process comes from the SM process $e^+e^- \rightarrow \nu \bar{\nu} \gamma$ and from the supersymmetric process $e^+e^- \rightarrow \tilde{\nu} \tilde{\nu}^* \gamma$.

The purpose of the present work is to establish the use of longitudinal beam polarization in probing the effects of boundary conditions in the neutralino sector that arise in GUTs at a linear collider. This is motivated by the fact that longitudinal polarization is a distinct possibility at the ILC. For the signal process considered, the dominant SM background comes from the radiative neutrino production process, which proceeds through the exchange of W bosons, which couple only to the left-handed particles. This dominant background made it difficult to observe the signal process at the LEP even for very light neutralinos. At the LHC also the CMS experiment has searched for a final state containing a photon and missing transverse energy, and the observed event yield was seen to be in agreement with the standard model expectations. However, in the case of the ILC with the availability of beam polarization, a suitable choice of beam polarization $(e_R^- e_L^+)$ will significantly reduce the expected SM background. Therefore, the ILC, with the availability of beam polarization, will be a good place to look for the processes with a high-energy photon and large missing energy in the final state. At the future linear colliders, because of high luminosity, ISR and
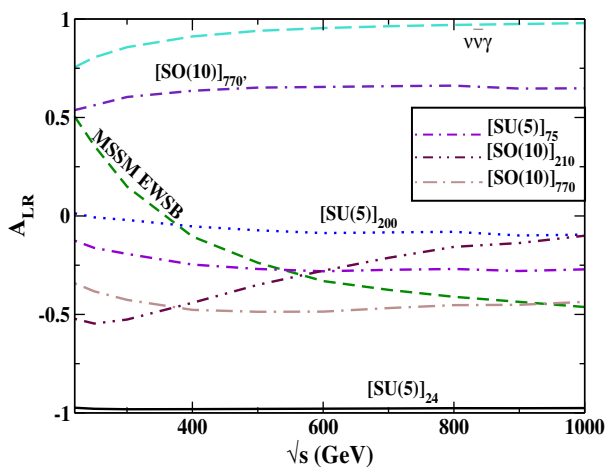
beamstrahlung are an unavoidable feature, and, therefore, we have included the radiative corrections in our calculations to obtain precise values for the cross sections.

We have studied in detail the cross section and the photon energy distribution for the signal and background process for a center-of-mass energy of 500 GeV and an integrated luminosity of 500 fb^{-1}. The initial beams are taken to be longitudinally polarized with $P_{e^-} = 0.8$ and $P_{e^+} = -0.6$. Our analyses show the behavior of the different models with the inclusion of beam polarization. Together with these the dependence of the cross section on the other free SUSY parameters which are involved in the signal process was also studied. This includes the $SU(2)_L$ gaugino mass parameter M_2 and the Higgs(ino) mass parameter μ as well as the selectron masses ($m_{\tilde{e}_R}, m_{\tilde{e}_L}$). Our results demonstrate that the composition of the lightest neutralino in different models plays a crucial role in the signal process. It can be seen from Table XVII how the bino- and wino-type neutralino production cross section will be controlled by different choices of initial beam polarization. Similarly the insensitivity of the Higgsino-type neutralino production cross section to the beam polarization, which is mediated through the Z boson, is also reflected in the table. For the bino-type neutralino, which arises in $SU(5)_{24}$, with significantly larger coupling to the right selectron, the cross section is increased with the choice of beam polarization used here, and the background is correspondingly reduced. At the same time in the case of other models, with the Higgsino-type lightest neutralino, there is no appreciable change in cross section for the choice of beam polarization used in this paper, since Z couples to both left- and right-handed fermions.

Finally, in order to study whether an excess of signal photons N_S can be observed over the background photons N_B from the SM radiative neutrino process, we have studied the theoretical statistical significance S and the signal-to-background ratio r. The dependence of S on the independent parameters M_2 and μ is also studied. The results that we have obtained emphasize the signal and the background cross sections along with the significance and the signal-to-background ratio for different degrees of initial beam polarization at different planned center-of-mass energies of the ILC. They are presented in Tables X, XI, and XII. Therefore, we conclude that in the presence of beam polarization with right-handed electrons and left-handed positrons, the models with a bino-type neutralino can be studied in detail through the radiative neutralino production it the ILC. In this respect the grand unified supersymmetric $SU(5)_{24}$ model is unique among all the models considered in this paper. In this case M_3 can be large so that we get the gluino mass satisfying the experimental constraints, and also M_1 will be small enough to lead to a light bino-type neutralino. Therefore, for the choice of parameters considered in our paper, $SU(5)_{24}$ will provide a signal which could be observed at the ILC. This provides a strong motivation for the search for the

radiative neutralino production as an evidence of a supersymmetric grand unified model at the ILC.

We would also like to point that even with initially polarized beams, the models with a Higgsino-type neutralino will be too difficult to be observed at the ILC. These Higgsino-type scenarios have a distinctive feature wherein $\tilde{\chi}_1^0$, $\tilde{\chi}_2^0$, and $\tilde{\chi}_1^\pm$ are almost degenerate with masses around μ due to large values of $M_{1,2}$ and a low value of μ. Due to the degeneracy in mass, the processes (a) $e^+ e^- \rightarrow \tilde{\chi}_1^0 \tilde{\chi}_2^0 \gamma$ and (b) $e^+ e^- \rightarrow \tilde{\chi}_2^0 \tilde{\chi}_2^0 \gamma$ will also yield a similar final state as the radiative neutralino production. A detailed study of signatures with a hard photon and large missing energy will include processes a and b along with the signal process considered here. This will result in a significant increase of cross section and may offer additional search avenues. We note here that $\tilde{\chi}_1^0 \tilde{\chi}_2^0$ and $\tilde{\chi}_2^0 \tilde{\chi}_2^0$ production channels tend to be suppressed, but may, nevertheless, offer increased search avenues. We do not consider this case any further here but leave it for a future publication.

APPENDIX A: GAUGINO MASSES IN GRAND UNIFIED THEORIES

In this section we review the nonuniversal and universal gaugino masses in grand unified theories.

1. Universal gaugino masses in grand unified theories

In supersymmetric models, with gravity mediated supersymmetry breaking, usually denoted as mSUGRA, the soft supersymmetry breaking gaugino mass parameters M_1, M_2, and M_3 satisfy the universal boundary conditions

$$M_1 = M_2 = M_3 = m_{1/2} \tag{A1}$$

at the grand unified scale M_G, where $i = 1, 2, 3$ refer to the $U(1)_Y$, $SU(2)_L$, and the $SU(3)_C$ gauge groups, respectively. Furthermore, the three gauge couplings corresponding to these gauge groups satisfy ($\alpha_i = g_i^2/4\pi$, $i = 1, 2, 3$)

$$\alpha_1 = \alpha_2 = \alpha_3 = \alpha_G \tag{A2}$$

at the GUT scale M_G, where $g_1 = \frac{5}{3} g'$, $g_2 = g$, with g' and g as $U(1)_Y$, and $SU(2)_L$ gauge couplings, respectively, and g_3 is the $SU(3)_C$ gauge coupling. The renormalization

group equations then imply that imply that out of three gaugino mass parameters, only one is independent, which we are free to choose as the gluino mass $M_3 \equiv M_{\tilde{g}}$. For the gaugino mass parameters, this leads to the ratio

$$M_1:M_2:M_3 \simeq 1:2:7.1. \qquad (A3)$$

The gaugino mass parameters described above are the running masses evaluated at the electroweak scale M_Z. A lower bound is then obtained on the parameter M_1 in the case of mSUGRA, from the constraint on M_2 (2.3) and the ratio (A3):

$$M_1 \gtrsim 50 \text{ GeV}. \qquad (A4)$$

2. Nonuniversal gaugino masses in grand unified theories

In contrast to the Sec. A 1 with universal boundary condition (A1) for the gaugino mass parameters at the GUT scale, we now consider the case of MSSM with nonuniversal boundary conditions at the GUT scale, which arise in $SU(5)$ and $SO(10)$ grand unified theories. Since in supersymmetric GUTs the gaugino masses need not be equal at the GUT scale, the neutralino masses and mixing can be different in SUSY GUTs as compared to the MSSM with universal gaugino masses.

The coupling of the field strength superfield W^a with the gauge kinetic function $f(\Phi)$ results in the generation of soft gaugino masses in supersymmetric models (see Ref. [28] and references therein). This term can be written as

$$\mathcal{L}_{\text{g.k.}} = \int d^2\theta f_{ab}(\Phi) W^a W^b + \text{H.c.,} \qquad (A5)$$

with a and b referring to gauge group indices and repeated indices being summed over. The gauge kinetic function $f_{ab}(\Phi)$ can be written in terms of the singlet and nonsinglet chiral superfields.

When the auxiliary part F_Φ of a chiral superfield Φ in $f(\Phi)$ gets a VEV $\langle F_\Phi \rangle$, the interaction (A5) gives rise to soft gaugino masses:

$$\mathcal{L}_{\text{g.k.}} \supset \frac{\langle F_\Phi \rangle_{ab}}{M_P} \lambda^a \lambda^b + \text{H.c.,} \qquad (A6)$$

where $\lambda^{a,b}$ are gaugino fields. Here λ^1, λ^2, and λ^3 are the $U(1)$, $SU(2)$, and $SU(3)$ gaugino fields, respectively. Since the gauginos belong to the adjoint representation of the gauge group, Φ and F_Φ can belong to any of the representations appearing in the symmetric product of the two adjoint representations of the corresponding gauge group. We note that in four-dimensional grand unified theories, only the gauge groups $SU(5)$, $SO(10)$, and E_6 support the chiral structure of weak interactions. Here we shall study the implications of nonuniversal gaugino masses for the case of $SU(5)$ and $SO(10)$ grand unified gauge groups.

a. $SU(5)$

In this section we shall consider the case where the SM gauge group is embedded in the grand unified gauge group $SU(5)$. For the symmetric product of the two adjoint (**24**-dimensional) representations of $SU(5)$, we have

$$(\mathbf{24} \otimes \mathbf{24})_{\text{Symm}} = \mathbf{1} \oplus \mathbf{24} \oplus \mathbf{75} \oplus \mathbf{200}. \qquad (A7)$$

In the simplest case where Φ and F_Φ are assumed to be in the singlet representation of $SU(5)$, we have equal gaugino masses at the GUT scale. But, as is obvious from Eq. (A7), Φ and F_Φ can belong to any of the nonsinglet representations **24**, **75**, and **200** of $SU(5)$. In such cases the soft gaugino masses are unequal but related to one another via the representation invariants of the gauge group [20]. In Table XIII we show the ratios of gaugino masses which result when F_Φ belong to different representations of $SU(5)$ in the decomposition (A8). In this paper, for definiteness, we shall study the case of each representation independently, although an arbitrary combination of these is also allowed.

In the one-loop approximation, the solution of renormalization group equations for the soft supersymmetry breaking gaugino masses M_1, M_2, and M_3 can be written as [76]

$$\frac{M_i(t)}{\alpha_i(t)} = \frac{M_i(\text{GUT})}{\alpha_i(\text{GUT})}, \qquad i = 1, 2, 3. \qquad (A8)$$

Then at any arbitrary scale, we have

$$
\begin{aligned}
M_1 &= \frac{5}{3} \frac{\alpha}{\cos^2\theta_W} \left(\frac{M_1(\text{GUT})}{\alpha_1(\text{GUT})} \right), \\
M_2 &= \frac{\alpha}{\sin^2\theta_W} \left(\frac{M_2(\text{GUT})}{\alpha_2(\text{GUT})} \right), \\
M_3 &= \alpha_3 \left(\frac{M_3(\text{GUT})}{\alpha_3(\text{GUT})} \right).
\end{aligned}
\qquad (A9)
$$

b. $SO(10)$

For the case of $SO(10)$, we have for the product of two adjoint (**45**)-dimensional representations

$$(\mathbf{45} \times \mathbf{45})_{\text{Symm}} = \mathbf{1} \oplus \mathbf{54} \oplus \mathbf{210} \oplus \mathbf{770}. \qquad (A10)$$

In Table XIV we have shown the gaugino mass parameters for the different representations that arise in the symmetric product (A10) for the $SO(10)$ group. We note from

TABLE XIII. Ratios of the gaugino masses at the GUT scale in the normalization $M_1(\text{GUT}) = 1$ and at the electroweak scale in the normalization $M_1(\text{EW}) = 1$ for F terms in different representations of $SU(5)$. These results are obtained by using 1-loop renormalization group equations.

$SU(5)$	M_1^G	M_2^G	M_3^G	M_1^{EW}	M_2^{EW}	M_3^{EW}
1	1	1	1	1	2	7.1
24	1	3	-2	1	6	-14.3
75	1	$-\frac{3}{5}$	$-\frac{1}{5}$	1	-1.18	-1.41
200	1	$\frac{1}{5}$	$\frac{1}{10}$	1	0.4	0.71

TABLE XIV. Ratios of the gaugino masses at the GUT scale in the normalization $M_1(\text{GUT}) = 1$ and at the electroweak scale in the normalization $M_1(\text{EW}) = 1$ for F terms in representations of $SU(5) \subset SO(10)$ with the normal (nonflipped) embedding. These results have been obtained at the 1-loop level.

$SO(10)$	$SU(5)$	M_1^G	M_2^G	M_3^G	M_1^{EW}	M_2^{EW}	M_3^{EW}
1	**1**	1	1	1	1	2	7.1
54	**24**	1	3	-2	1	6	-14.3
210	**1**	1	1	1	1	2	7.1
	24	1	3	-2	1	6	-14.3
	75	1	$-\frac{3}{5}$	$-\frac{1}{5}$	1	-1.18	-1.41
770	**1**	1	1	1	1	2	7.1
	24	1	3	-2	1	6	-14.3
	75	1	$-\frac{3}{5}$	$-\frac{1}{5}$	1	-1.18	-1.14
	200	1	$\frac{1}{5}$	$\frac{1}{10}$	1	0.4	0.71

TABLE XV. Ratios of the gaugino masses at the GUT scale in the normalization $M_1(\text{GUT}) = 1$ and at the electroweak scale in the normalization $M_1(\text{EW}) = 1$ at the 1-loop level for F terms in representations of flipped $SU(5)' \times U(1) \subset SO(10)$.

$SO(10)$	$[SU(5)' \times U(1)]_{\text{flipped}}$	M_1^G	M_2^G	M_3^G	M_1^{EW}	M_2^{EW}	M_3^{EW}
1	$(\mathbf{1}, 0)$	1	1	1	1	2	7.1
54	$(\mathbf{24}, 0)$	1	3	-2	1	6	-14.3
210	$(\mathbf{1}, 0)$	1	$-\frac{5}{19}$	$-\frac{5}{19}$	1	-0.52	-1.85
	$(\mathbf{24}, 0)$	1	$-\frac{15}{7}$	$\frac{10}{7}$	1	-4.2	10
	$(\mathbf{75}, 0)$	1	-15	-5	1	-28	-33.33
770	$(\mathbf{1}, 0)$	1	$\frac{5}{77}$	$\frac{5}{77}$	1	0.13	0.46
	$(\mathbf{24}, 0)$	1	$\frac{15}{101}$	$-\frac{10}{101}$	1	0.3	-0.70
	$(\mathbf{75}, 0)$	1	-15	-5	1	-28	-33.3
	$(\mathbf{200}, 0)$	1	5	$\frac{5}{2}$	1	9.33	16.67

TABLE XVI. Ratios of the gaugino masses at the GUT scale in the normalization $M_1(\text{GUT}) = 1$ and at the electroweak scale in the normalization $M_1(\text{EW}) = 1$ at the 1-loop level for F terms in representations of $SU(4) \times SU(2)_L \times SU(2)_R \subset SO(10)$.

$SO(10)$	$SU(4) \times SU(2)_R$	M_1^G	M_2^G	M_3^G	M_1^{EW}	M_2^{EW}	M_3^{EW}
1	$(\mathbf{1}, \mathbf{1})$	1	1	1	1	2	7.1
54	$(\mathbf{1}, \mathbf{1})$	1	3	2	1	6	-14.3
210	$(\mathbf{1}, \mathbf{1})$	1	$-\frac{5}{3}$	0	1	-3.35	0
	$(\mathbf{15}, \mathbf{1})$	1	0	$-\frac{5}{4}$	1	0	-9.09
	$(\mathbf{15}, \mathbf{3})$	1	0	0	1	0	0
770	$(\mathbf{1}, \mathbf{1})$	1	$\frac{25}{19}$	$\frac{10}{19}$	1	2.6	3.7
	$(\mathbf{1}, \mathbf{5})$	1	0	0	1	0	0
	$(\mathbf{15}, \mathbf{3})$	1	0	0	1	0	0
	$(\mathbf{84}, \mathbf{1})$	1	0	$\frac{5}{32}$	1	0	1.11

TABLE XVII. Vertices corresponding to different terms in the interaction Lagrangian (B4) for the MSSM. Here we have also shown the vertices for selectron-photon and electron-photon interactions [26].

Vertex	Vertex factor
right selectron— electron—neutralino	$\frac{-ie\sqrt{2}}{\cos\theta_w} N_{11}^* P_L$
left selectron— electron—neutralino	$\frac{ie}{\sqrt{2}\sin\theta_w}(N_{12} + \tan\theta_w N_{11})P_R$
neutralino—Z^0— neutralino	$\frac{ie}{4\sin\theta_w\cos\theta_w}(|N_{13}|^2 - |N_{14}|^2)\gamma^\mu\gamma^5$
electron—Z^0— electron	$ie\gamma^\mu[\frac{1}{\sin\theta_w\cos\theta_w}(\frac{1}{2} - \sin^2\theta_w)P_L - \tan\theta_w P_R]$
selectron—photon— selectron	$ie(p_1 + p_2)^\mu$
electron—photon— electron	$ie\gamma^\mu$

Table XIV that the ratios of gaugino masses for the different representations of $SO(10)$ in the symmetric product (A10) with the unflipped embedding $SU(5) \subset SO(10)$ are identical to the corresponding gaugino mass ratios in Table XIII for the embedding of SM in $SU(5)$. Therefore, the input parameters and the resulting masses for the gaugino mass ratios in Table XIV for $SO(10)$ are identical to the corresponding Tables II, III, and IV for $SU(5)$.

There are two additional maximal power subgroups of $SO(10)$, consistent with fermion content of the SM, apart from $SU(5) \subset SO(10)$. We, therefore, list in Tables XV and XVI, the ratio of the gaugino mass parameters, both at the GUT and electroweak scale, for different representations that arise in the symmetric product of two adjoint representations of $SO(10)$ with relevant embedding of these subgroups in $SO(10)$.

APPENDIX B: NEUTRALINO MASS MATRIX, LAGRANGIAN, AND COUPLINGS

In this Appendix we recall the mixing matrix for the neutralinos and the couplings that enter our calculations of the radiative neutralino cross section. We note that the neutralino mass matrix receives contribution from MSSM superpotential term

$$W_{\text{MSSM}} = \mu H_1 H_2, \qquad (B1)$$

where H_1 and H_2 are the Higgs doublet chiral superfields with opposite hypercharge and μ is the supersymmetric Higgs(ino) mass parameter. In addition to Eq. (B1), the neutralino mass matrix receives contributions from the interactions between gauge and matter multiplets as well as contributions from the soft supersymmetry breaking masses for the $SU(2)_L$ and $U(1)_Y$ gauginos. Putting together all these contributions, the neutralino mass matrix, in the bino, wino, higgsino basis $(-i\lambda', -i\lambda^3, \psi_{H_1}^1, \psi_{H_2}^2)$, can be written as [2,57]

$$M_{\text{MSSM}} = \begin{pmatrix} M_1 & 0 & -m_Z \sin\theta_W \cos\beta & m_Z \sin\theta_W \sin\beta \\ 0 & M_2 & m_Z \cos\theta_W \cos\beta & -m_Z \cos\theta_W \sin\beta \\ -m_Z \sin\theta_W \cos\beta & m_Z \cos\theta_W \cos\beta & 0 & -\mu \\ m_Z \sin\theta_W \sin\beta & -m_Z \cos\theta_W \sin\beta & -\mu & 0 \end{pmatrix}, \tag{B2}$$

where M_1 and M_2 are the $U(1)_Y$ and the $SU(2)_L$ soft gaugino mass parameters, respectively, and $\tan\beta = v_2/v_1$ is the ratio of the vacuum expectation values of the neutral components of the two Higgs doublet fields H_1 and H_2, respectively. Furthermore, m_Z is the Z boson mass, and θ_W is the weak mixing angle. In our analyses we are considering all parameters in the neutralino mass matrix to be real. In this case it can be diagonalised by an orthogonal matrix. If one of the eigenvalues of M_{MSSM} is negative, then we can diagonalize this matrix using a

unitary matrix N, the neutralino mixing matrix, to get a positive semidefinite diagonal matrix [57] with the neutralino masses $m_{\chi_i^0}$ ($i = 1, 2, 3, 4$) in order of increasing value:

$$N^* M_{\text{MSSM}} N^{-1} = \text{diag}(m_{\chi_1^0}, m_{\chi_2^0}, m_{\chi_3^0}, m_{\chi_4^0}). \tag{B3}$$

For the minimal supersymmetric standard model, the interaction Lagrangian of neutralinos, electrons, selectrons, and Z bosons is summarized by [57]

$$\mathcal{L} = \left(-\frac{\sqrt{2}e}{\cos\theta_W} N_{11}^*\right) \bar{f}_e P_L \tilde{\chi}_1^0 \tilde{e}_R + \frac{e}{\sqrt{2}\sin\theta_W}(N_{12} + \tan\theta_W N_{11}) \bar{f}_e P_R \tilde{\chi}_1^0 \tilde{e}_L + \frac{e}{4\sin\theta_W \cos\theta_W}(|N_{13}|^2 - |N_{14}|^2) Z_\mu \bar{\tilde{\chi}}_1^0 \gamma^\mu \gamma^5 \tilde{\chi}_1^0$$
$$+ e Z_\mu \bar{f}_e \gamma^\mu \left[\frac{1}{\sin\theta_W \cos\theta_W}\left(\frac{1}{2} - \sin^2\theta_W\right) P_L - \tan\theta_W P_R\right] f_e + \text{H.c.}, \tag{B4}$$

with the electron, selectrons, neutralino, and Z boson fields denoted by f_e, $\tilde{e}_{L,R}$, $\tilde{\chi}_1^0$, and Z_μ, respectively, and $P_{R,L} = \frac{1}{2}(1 \pm \gamma^5)$. The interaction vertices arising from Eq. (B4) are summarized in Table XVII.

[1] H. P. Nilles, Phys. Rep. **110**, 1 (1984); P. Nath, R. L. Arnowitt, and A. H. Chamseddine, http://ccdb5fs.kek.jp/cgi-bin/img/allpdf?198402095.

[2] A. Bartl, H. Fraas, W. Majerotto, and N. Oshimo, Phys. Rev. D **40**, 1594 (1989).

[3] A. Bartl, H. Fraas, and W. Majerotto, Nucl. Phys. **B278**, 1 (1986).

[4] P. N. Pandita, Phys. Rev. D **50**, 571 (1994).

[5] P. N. Pandita, Z. Phys. C **63**, 659 (1994).

[6] P. N. Pandita, Phys. Rev. D **53**, 566 (1996).

[7] P. N. Pandita, arXiv:hep-ph/9701411.

[8] S. Y. Choi, J. Kalinowski, G. A. Moortgat-Pick, and P. M. Zerwas, Eur. Phys. J. C **22**, 563 (2001); **23**, 769(E) (2002).

[9] K. Huitu, J. Laamanen, and P. N. Pandita, Phys. Rev. D **67**, 115009 (2003).

[10] K. Huitu, J. Laamanen, P. N. Pandita, and P. Tiitola, Phys. Rev. D **82**, 115003 (2010).

[11] J. A. Aguilar-Saavedra et al. (ECFA/DESY LC Physics Working Group), arXiv:hep-ph/0106315.

[12] T. Abe et al. (American Linear Collider Working Group), in Proceedings of the APS/DPF/DPB Summer Study on the Future of Particle Physics, Snowmass, CO, 2001, edited by N. Graf.

[13] K. Abe et al. (ACFA Linear Collider Working Group), arXiv:hep-ph/0109166.

[14] G. Weiglein et al. (LHC/LC Study Group), Phys. Rep. **426**, 47 (2006).

[15] J. A. Aguilar-Saavedra et al., Eur. Phys. J. C **46**, 43 (2006).

[16] G. A. Moortgat-Pick et al., Phys. Rep. **460**, 131 (2008).

[17] E. Cremmer, S. Ferrara, L. Girardello, and A. Van Proeyen, Phys. Lett. **116B**, 231 (1982).

[18] L. Randall and R. Sundrum, Nucl. Phys. **B557**, 79 (1999); G. F. Giudice, M. A. Luty, H. Murayama, and R. Rattazzi, J. High Energy Phys. 12 (1998) 027.

[19] K. Huitu, J. Laamanen, and P. N. Pandita, Phys. Rev. D **65**, 115003 (2002).

[20] J. R. Ellis, K. Enqvist, D. V. Nanopoulos, and K. Tamvakis, Phys. Lett. **155B**, 381 (1985); M. Drees, Phys. Lett. **158B**, 409 (1985); G. Anderson, C. H. Chen, J. F. Gunion, J. D. Lykken, T. Moroi, and Y. Yamada, in Proceedings of 1996 DPF/DPB Summer Study on New Directions for High-Energy Physics, Snowmass, CO, 1996.

[21] V. D. Barger and C. Kao, Phys. Rev. D **60**, 115015 (1999); G. Anderson, H. Baer, C.-H. Chen, and X. Tata, Phys. Rev. D **61**, 095005 (2000).

[22] K. Huitu, Y. Kawamura, T. Kobayashi, and K. Puolamäki, Phys. Rev. D **61**, 035001 (1999); G. Bélanger, F. Boudjema, A. Cottrant, A. Pukhov, and A. Semenov, Nucl. Phys. **B706**, 411 (2005).

[23] A. Djouadi, Y. Mambrini, and M. Muhlleitner, Eur. Phys. J. C **20**, 563 (2001).

[24] V. Bertin, E. Nezri, and J. Orloff, J. High Energy Phys. 02 (2003) 046; A. Birkedal-Hansen and B. D. Nelson, Phys.

Rev. D **67**, 095006 (2003); U. Chattopadhyay and D. P. Roy, Phys. Rev. D **68**, 033010 (2003).

[25] A. Corsetti and P. Nath, Phys. Rev. D **64**, 125010 (2001).

[26] R. Basu, P. N. Pandita, and C. Sharma, Phys. Rev. D **77**, 115009 (2008).

[27] P. N. Pandita and C. Sharma, Phys. Rev. D **85**, 015021 (2012).

[28] P. N. Pandita and M. Patra, Int. J. Mod. Phys. A **27**, 1250172 (2012).

[29] C. Bartels, O. Kittel, U. Langenfeld, and J. List, arXiv:1202.6324.

[30] J. R. Ellis, J. M. Frere, J. S. Hagelin, G. L. Kane, and S. T. Petcov, Phys. Lett. **132B**, 436 (1983); E. Reya, Phys. Lett. **133B**, 245 (1983); P. Chiappetta, J. Soffer, P. Taxil, F. M. Renard, and P. Sorba, Nucl. Phys. **B262**, 495 (1985); **B279**, 824(E) (1987).

[31] P. Fayet, Phys. Lett. **117B**, 460 (1982).

[32] J. R. Ellis and J. S. Hagelin, Phys. Lett. **122B**, 303 (1983).

[33] K. Grassie and P. N. Pandita, Phys. Rev. D **30**, 22 (1984).

[34] T. Kobayashi and M. Kuroda, Phys. Lett. **139B**, 208 (1984).

[35] J. D. Ware and M. E. Machacek, Phys. Lett. **142B**, 300 (1984).

[36] L. Bento, J. C. Romao, and A. Barroso, Phys. Rev. D **33**, 1488 (1986).

[37] M. Chen, C. Dionisi, M. Martinez, and X. Tata, Phys. Rep. **159**, 201 (1988).

[38] T. Kon, Prog. Theor. Phys. **79**, 1006 (1988).

[39] S. Y. Choi, J. S. Shim, H. S. Song, J. Song, and C. Yu, Phys. Rev. D **60**, 013007 (1999).

[40] A. Datta, A. Datta, and S. Raychaudhuri, Eur. Phys. J. C **1**, 375 (1998); Phys. Lett. B **349**, 113 (1995).

[41] S. Ambrosanio, B. Mele, G. Montagna, O. Nicrosini, and F. Piccinini, Nucl. Phys. **B478**, 46 (1996).

[42] A. Heister *et al.* (ALEPH Collaboration), Eur. Phys. J. C **28**, 1 (2003).

[43] J. Abdallah *et al.* (DELPHI Collaboration), Eur. Phys. J. C **38**, 395 (2005).

[44] P. Achard *et al.* (L3 Collaboration), Phys. Lett. B **587**, 16 (2004).

[45] G. Abbiendi *et al.* (OPAL Collaboration), Eur. Phys. J. C **29**, 479 (2003).

[46] G. Abbiendi *et al.* (OPAL Collaboration), Eur. Phys. J. C **18**, 253 (2000).

[47] H. K. Dreiner, O. Kittel, and U. Langenfeld, Eur. Phys. J. C **54**, 277 (2008).

[48] K. J. F. Gaemers, R. Gastmans, and F. M. Renard, Phys. Rev. D **19**, 1605 (1979).

[49] S. Chatrchyan *et al.* (CMS Collaboration), Phys. Rev. Lett. **108**, 261803 (2012).

[50] LEPSUSYWG, ALEPH, DELPHI, L3, and OPAL experiments, Report No. LEPSUSYWG/01-03.1 (http://lepsusy.web.cern.ch/lepsusy/Welcome.html).

[51] W. M. Yao *et al.* (Particle Data Group), J. Phys. G **33**, 1 (2006).

[52] J. Abdallah *et al.* (DELPHI Collaboration), Eur. Phys. J. C **31**, 421 (2003).

[53] H. K. Dreiner, S. Heinemeyer, O. Kittel, U. Langenfeld, A. M. Weber, and G. Weiglein, Eur. Phys. J. C **62**, 547 (2009).

[54] ATLAS Collaboration, Report No. ATLAS-CONF-2012-033, 2012.

[55] CMS Collaboration, Report No. CMS-PAS-SUS-12-005, 2012.

[56] CMS Collaboration, Report No. CMS-PAS-SUS-11-020, 2011.

[57] H. E. Haber and G. L. Kane, Phys. Rep. **117**, 75 (1985).

[58] A. Pukhov, arXiv:hep-ph/0412191.

[59] S. Eidelman *et al.* (Particle Data Group), Phys. Lett. B **592**, 1 (2004).

[60] E. A. Kuraev and V. S. Fadin, Yad. Fiz. **41**, 733 (1985) [Sov. J. Nucl. Phys. **41**, 466 (1985)].

[61] O. Nicrosini and L. Trentadue, Phys. Lett. B **196**, 551 (1987).

[62] M. Skrzypek and S. Jadach, Z. Phys. C **49**, 577 (1991).

[63] R. Blankenbecler and S. D. Drell, Phys. Rev. D **36**, 277 (1987).

[64] J. Brau *et al.*, Report No. ILC-REPORT-2007-001.

[65] H. K. Dreiner, O. Kittel, and U. Langenfeld, Phys. Rev. D **74**, 115010 (2006).

[66] A. Djouadi, J.-L. Kneur, and G. Moultaka, Comput. Phys. Commun. **176**, 426 (2007).

[67] C. H. Chen, M. Drees, and J. F. Gunion, Phys. Rev. Lett. **76**, 2002 (1996).

[68] F. A. Berends, G. J. H. Burgers, C. Mana, M. Martinez, and W. L. van Neerven, Nucl. Phys. **B301**, 583 (1988).

[69] F. Boudjema *et al.*, arXiv:hep-ph/9601224.

[70] G. Montagna, M. Moretti, O. Nicrosini, and F. Piccinini, Nucl. Phys. **B541**, 31 (1999).

[71] F. Franke and H. Fraas, Phys. Rev. D **49**, 3126 (1994).

[72] H. E. Haber and D. Wyler, Nucl. Phys. **B323**, 267 (1989).

[73] S. Ambrosanio and B. Mele, Phys. Rev. D **53**, 2541 (1996).

[74] S. Ambrosanio and B. Mele, Phys. Rev. D **55**, 1399 (1997); [**56**, 3157 (1997)].

[75] H. Baer and T. Krupovnickas, J. High Energy Phys. 09 (2002) 038.

[76] S. P. Martin and P. Ramond, Phys. Rev. D **48**, 5365 (1993).